VORTEX VALVE EXHAUST-DRIVEN PRESSURE OSCILLATIONS IN HYBRID COMBUSTION

by

STEPHEN C. BATES

S.B., Massachusetts Institute of Technology
(1970)

Submitted in Partial Fulfillment

of the Requirements for the

Degree of Master of Science

at the

Massachusetts Institute of Technology

June 1971

Signature of Author _____
Department of Aeronautics and
Astronautics, June 1971

Certified by _____
Thesis Supervisor

Accepted by _____
Chairman, Departmental
Graduate Committee

VORTEX VALVE EXHAUST-DRIVEN PRESSURE OSCILLATIONS IN HYBRID COMBUSTION

by

Stephen C. Bates

Submitted to the Department of Aeronautics and Astronautics in June 1971, in partial fulfillment of the requirements for the degree of Master of Science.

ABSTRACT

This was primarily an experimental thesis. There were two goals. The first was to see if the chamber pressure of a burning rocket could be forced to oscillate at a given frequency by using a vortex valve to control the exhaust. The second was to study some predicted pressure instabilities of hybrid combustion, both by themselves and using the vortex valve to study any resonance behaviors.

A small plexiglas-oxygen hybrid vurner was used, and the regression rate was concluded to be convective heat transfer limited with radiation effects at lower flow rates. Vortex valve chamber pressure driving was found to be practical, although limited mechanically in this case. Resonance amplitude driving was not achieved.

Inherent pressure oscillations in the hybrid used are concluded to be caused by non-equilibrium vapor pressure-regression rate coupling after a consideration of a number of different models. These oscillations are found not to be mass flow rate dependent.

Thesis Advisor: David B. Stickler

Title: Assistant Professor of Aeronautics and Astronautics

ACKNOWLEDGEMENTS

Thanks go to Mr. Thorwald Christensen, Mr. Kenneth Griffith, and Mr. Roy Andrew who provided expert mechanical advice innumerable times, and to my advisor Professor David B. Stickler who provided almost all of the ideas incorporated in this thesis. Also thanks to myself for making a small number of not previously accepted conclusions.

SYMBOLS

A	Area
A_b	Burning area
B	Blowing factor $= \dfrac{(\rho v)_w}{\rho_e u_e C_f/2}$
C^*	Characteristic velocity $= \sqrt{\dfrac{RT}{\gamma M}} \left(\dfrac{\gamma + 1}{2}\right)^{\frac{\gamma + 1}{2(\gamma - 1)}}$
C_f	Skin friction coefficient
C_{f_o}	Skin friction coefficient without mass addition
C_p	Specific heat at constant pressure
C_v	Specific heat at constant volume
d	Diameter
d_v	Vortex valve cavity diameter
G	Mass flow rate per unit area
g	Acceleration of gravity at the earth's surface
h	Enthalpy
h_v	Latent heat of vaporization
Δh	Enthalpy difference between flame and wall
K	Mass fraction
°K	Degrees Kelvin
k	Thermal conductivity
l	Length
L	Burning length
L^*	Characteristic length
Le	Lewis number $= \dfrac{\rho D \bar{C}_p}{K}$
$\dot{m}$	Mass flow rate
M_L	Mass loss from fuel charge

Symbols continued

M	Molecular weight
n	Vortex valve cavity thickness
p-p	Peak to peak pressure amplitude
p	Pressure
Pr	Prandl number = $\frac{\mu C_p}{k}$
$\dot{q}$	Heat flux per unit area
R	Effective vortex valve gas circumference radius
R	Universal gas constant
$\dot{r}$	Heat flux per unit aera
$\bar{\dot{r}}$	Averaged regression rate
Re_x	Reynolds number based on length = $\frac{\rho u x}{\mu}$
T	Temperature
u	Velocity parallel to wall
v	Velocity normal to wall
V	Volume
w	Weight
x	Distance parallel to wall
y	Distance normal to wall
δ	Boundary layer thickness
ε	Emissivity
γ	C_p/C_v
ρ	Density
σ	Stefan-Boltzmann constant
μ	Coefficient of viscosity

Subscripts

-	Average
b	Flame
c	Chamber
cf	Control flow
e	Free stream
f	Fuel
g	Gas
He	Helium
o	Stagnation
ox	Oxygen
s	Interior solid
t	Throat
v	Vortex valve

TABLE OF CONTENTS

Figures cont'd

Tables

CHAPTER I

INTRODUCTION

There are two basic purposes for this thesis. One is to investigate and hopefully explain existing pressure instabilities in an operating hybrid rocket; the other is to discover if it is possible to force the rocket's chamber pressure to oscillate at a chosen frequency by using a vortex valve attached to the exhaust, and then see if this can be used to drive the instability at resonance.

A hybrid rocket has a number of qualities that make it a good device for what we are doing. Using fairly low specific impulse fuels, such as the plexiglas-oxygen combination used here, results in a very safe system compared with either liquid or solid propellant rockets. The reason for this is the phenomenon of diffusion controlled boundary layer combustion, which makes a detonable mixture in the chamber very unlikely. Another advantage of using a hybrid is the lack of an accepted theory for the various regimes of operation. It is thought that perhaps the study here on pressure instabilities may shed some light on the various existing models. Plexiglas-oxygen is used in particular because of the large amount of study that has been done on it.

The models that are in use at present have arisen out of the heat transfer limited model, such as that developed by Marxman et al.,[5,6,7,10] and the experimental divergences from this model. The results of the heat transfer limited model in terms of a burning rate equation are fairly well accepted and agree with experiments within bounds, but the models differ somewhat from case to case. Models for other modes of hybrid combustion

are under debate at this writing. The following chapter discusses the heat transfer limited model and a number of the other "reasonable" models for other regions of operation. The models considered are those thought to be useful in explaining the possible pressure instabilities in hybrids. The author knows of no other hybrid instability studies.

The advantages of using a vortex valve to drive chamber pressure oscillations are more obvious. The main one is that it uses no mechanical devices that would be in contact with the hot flow and this eliminates many material problems. Control is obtained by adding a modulated cold flow tangentially to the combustion products from the combustion chamber. Theoretical understanding of the operation of a vortex valve is given by Lewellen et al.[4]. Investigation has also been done on using a vortex valve for modulation of solid rockets by Walsh.[11] Here the valve was used as a true dynamic device for controlling the chamber pressure. A dynamic analysis was not attempted here, and this is just one area in need of further study.

Chapter III describes the design and construction of the hybrid rocket and vortex valve with a brief explanation of vortex valve operation. Chapter IV explains the experiments that were done and the motivations involved in them. Chapter V gives results of basic hybrid combustion tests and the effectiveness of the vortex valve as a driver for chamber pressure oscillations. Data correlation with models discussed in chapter I is also given. Chapter VI consists of proposed models that might explain the observed hybrid instability. Some conclusions are made about this on the basis of experiments done here and more experiments are proposed to further clarify the issue.

CHAPTER II

STEADY STATE HYBRID THEORY

The basic model of hybrid combustion at present is that of heat transfer limited burning. It is considered at depth by Marxman et al [3,4,5,6] and what is presented in this paper is primarily taken from these works.

The model is built around the assumption that the rate of wall vaporization is determined solely by the heat transferred to the wall,

$$\dot{q}_w = \bar{\dot{r}}\, \rho_f\, h_v \tag{2.1}$$

where $\bar{\dot{r}}$ is a time averaged regression rate. Burning takes place (in this model) in a thin flame zone close to the wall, inside the boundary layer, beneath a free stream of oxidizer. Both the fuel and oxidizer are transported through the boundary layer. Thin, in this case, is defined as small compared to the boundary layer thickness.

The next step is the mechanism of heat transfer from the flame zone. The two modes considered are convection and radiation, the latter usually taken as the smaller of the two. Radiation is by far the simpler of the two and is written adequately just as black body radiation.

$$\dot{q}_r = \sigma\, \varepsilon_w\, (\varepsilon_g T_b^4 - T_w^4) \tag{2.2}$$

The point to note here is the very weak dependence on the boundary layer properties through the gas emissivity ε_g.

Heat convection through the gas between the flame and the wall is analysed by use of Reynolds analogy, which states that the momentum and

enthalpy profiles are similar as a function of height in the boundary layer.

$$-\frac{\dot{q}}{dh/dy} = \frac{\tau}{du/dy} \qquad (Pr = 1,\ Le = 1) \tag{2.3}$$

or

$$\frac{\dot{q}_w}{\Delta h} = \frac{\tau_w}{u_b} \qquad (\dot{q}_r = 0) \tag{2.4}$$

This is found to be valid even for combusting boundary layers. The object is to relate this to an empirically known skin friction coefficient.

$$C_f/2 \equiv \frac{\tau_w}{\rho_e u_e^2} \tag{2.5}$$

At this point life is complicated by the inclusion of mass addition at the wall. We define a blowing factor, B, by;

$$B = \frac{(\rho v)_w}{\rho_e u_e C_f/2} \tag{2.6}$$

The ratio C_f/C_{f_o} is then a function of this blowing factor B.

$$C_f/C_{f_o} = \frac{\ln(1+B)}{B} \qquad B < 5 \quad \text{(thin film approximation)} \tag{2.7}$$

$$C_f/C_{f_o} \simeq 1.2\, B^{-0.77} \qquad 5 < B < 100 \quad \text{(curve fit)} \tag{2.8}$$

Existence of mass addition also has an effect on the behavior of the boundary layer. Mass addition lowers the transition (laminar to turbulent) Reynolds number to 10^4 (perhaps even 10^3) so the boundary layers become turbulent very near the leading edge.

For turbulent flow, C_{f_o} is given empirically by:

$$C_{f_o}/2 = .03 \; R_{e_x}^{-0.2} \tag{2.9}$$

Putting equations (2.1), (2.4), (2.5) and (2.9) together (with $G_e \equiv \rho_e u_e$, $\dot{q}_r = 0$),

$$\bar{\dot{r}}\, \rho_f = .03 \; R_{e_x}^{-0.2} \; G_e \; C_f/C_{f_o} \; \frac{\Delta h}{h_v} \frac{u_e}{u_b} \tag{2.10}$$

The quantity $\frac{\Delta h}{h_v} \frac{u_e}{u_b}$ is a thermochemical mass addition parameter which forms an upper limit on B in practical systems.

$$\frac{\Delta h}{h_v} \frac{u_e}{u_b} \equiv B' = Pr^{0.67} \; B \tag{2.11}$$

If we now put equations (2.8) and (2.11) into (2.10) we get the standard burning rate equation presented by Marxman et al.

$$\rho_f \bar{\dot{r}} = 0.036 \; G \; B^{0.23} \; R_{e_x}^{-0.2} \qquad (Pr = 1) \tag{2.12}$$

Since supposedly B' will be fixed for a given fuel-oxidizer system the above relation states:

$$\bar{\dot{r}} \propto G^{0.8} \tag{2.13}$$

Radiation is included by noting that for a given increase in radiant heat flow the mass addition at the wall increases and the convective heat flow decreases. Thus the approximation,

$$\rho_f \bar{\dot{r}} = \frac{\dot{q}_c}{h_v} \left[e^{\dot{q}_r/\dot{q}_c} + \dot{q}_r/q_c \right] \tag{2.14}$$

and the conclusion that the effects exactly balance for $\dot{q}_r/q_c$ small, so that it is valid to use just $\dot{q}_c$ for typical hybrids.

The flame position and approximate velocity profile can also be developed in this model, given a fuel stoichiometry. An additional assumption, used to approximate the flame zone location, is an infinitely thin flame zone (infinite reaction rates).

The various profiles describing this model are presented in figure 1. The behavior of these parameters is enough to specify the major aspects of the heat transfer limited model.

At this point I will begin to be concerned with newer developments.

The heat transfer limited model works well for certain regimes of G and chamber pressure, depending on the fuel-oxidizer combination chosen. However, differences from experiment are found on both sides of this regime, at values other than the limits predicted by the theory itself.

Smoot and Price[6] have looked at both divergences and suggested various explanations. Stickler and Kumar[8] have specifically investigated the mechanism at high P_c and high G.

The trouble that occurs is that at both high and low G, chamber pressure dependencies are seen, while the heat transfer limited model predicts no such behavior. As stated often in the model, chemical kinetics have been assumed not to be important. This omission is what is explored by Stickler and Kumar to explain the behavior for high G and P_c. Apparently the main reason for initially neglecting chemical kinetics was the fundamental work of Lees[2] on convective heat transfer with mass addition and combustion. His conclusion was that the enthalpy difference between the flame and the wall is independent to first order of the detailed reaction kinetics.

Before going on, let me introduce "realistic" parameter profiles as

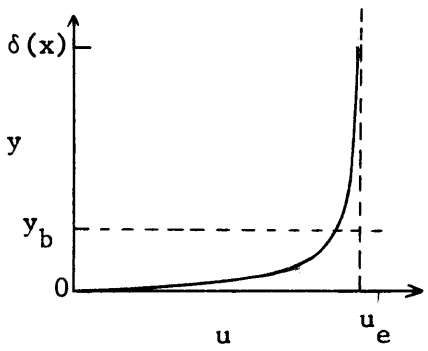

(a) Velocity

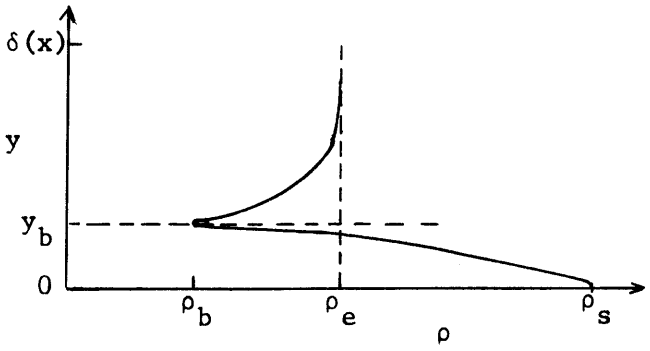

(b) Density

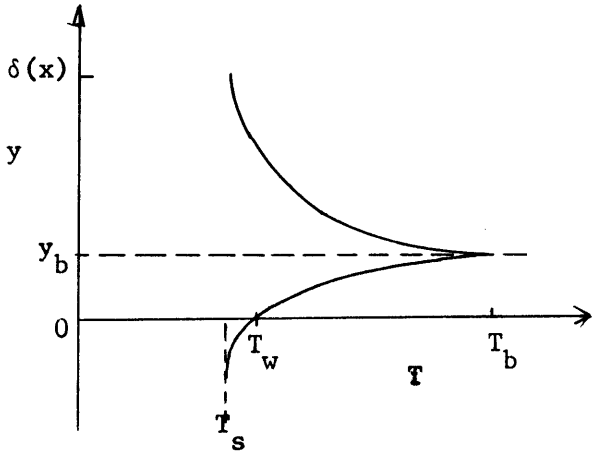

(c) Temperature

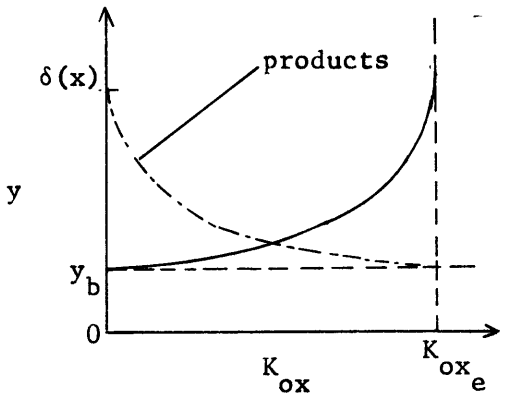

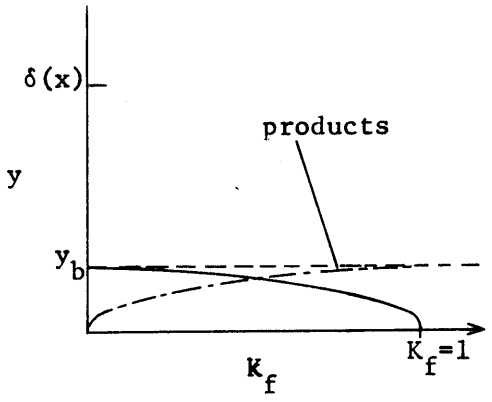

(d) Concentration

Figure 1 Heat Transfer Limited Model Profiles

shown in figure 2. These profiles employ a number of assumptions. One is a favorable pressure gradient down the length of the grain,which results in the velocity overshoot in the flame zone. This is a basic deduction from Bernoulli's law along a streamline, coupled with the fact that the stagnation enthalpy is constant along the streamline. This last "fact" can be seen to be reasonable if the flame height is at a constant fraction of the boundary layer height, as is concluded from diffusion arguments and constant flame stoichiometry. The other major assumption is the existence of finite concentrations (time averaged) of both fuel and oxidizer throughout the boundary layer. This assumption is supported by measurements taken by Kumar[1] and others[10] of wall oxidizer concentrations for hybrid systems. The existence of finite concentrations of fuel and oxidizer are predicted by a larger than molecular scale eddy model of turbulence, where unburned eddies can pass directly through the "flame zone" due to the inherently unsteady aspect of turbulence, and appear as finite time averaged concentrations. The only other difference from the heat transfer limited model profiles is that of a finite flame zone thickness of perhaps 10% of the boundary layer height. This has also been observed by myself among others for hybrid burners.

The concentration assumption is one required by the pressure sensitive model proposed by Stickler and Kumar. They consider the polymer degradation of the fuel to be the rate controlling process. The chamber pressure dependence enters into the model by the wall concentration of oxidizer functioning as a catalytic agent in the depolymerization process and thereby controlling the polymer vaporization rate for a given heat input. Details of the model are not relevant to the present discussion

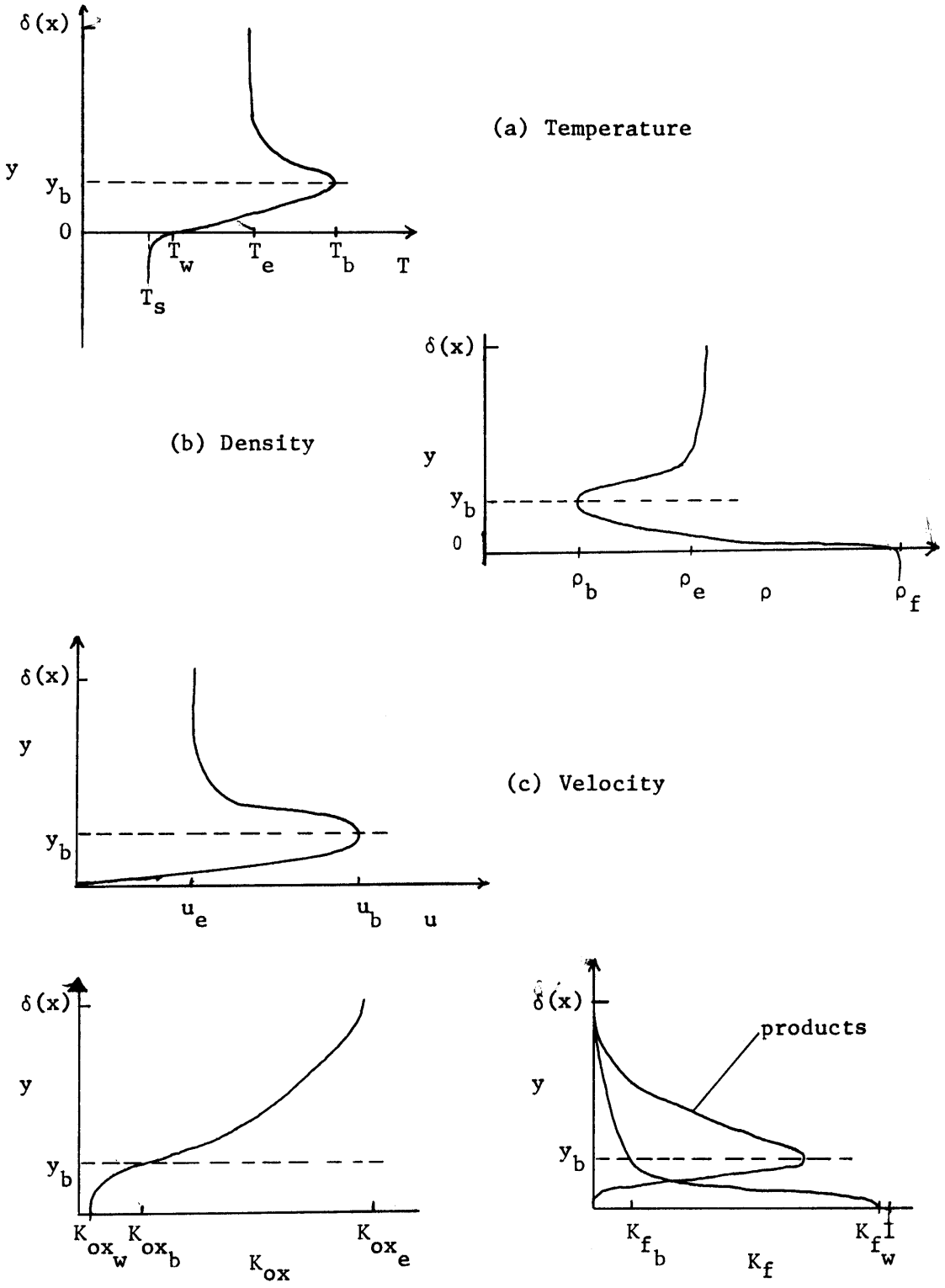

Figure 2 Boundary Layer with Combustion - qualitative parameter profiles

with one exception. That is their model of polymer vaporization and the boundary condition at the wall. The boundary condition they used was vapor pressure equilibrium of each polymer fragment vaporizing larger than monomer. Their conclusion was that the average chain length vaporizing was not monomer but approximately 6 monomer units. This vaporizing particle size is expected to be pressure dependent as well as being heat transfer dependent. Overall, their model predicts a burning rate dependence directly proportional to the partial pressure of oxidizer at the wall, and thence to chamber pressure.

$$\dot{r} \propto p_{ox_w} \propto p_c \tag{2.15}$$

Smoot and Price[7] consider a number of pressure sensitive mechanisms. They state that radiative heat transfer becomes a significant correction to the convective transfer for a B of 5 and above. They also claim that radiative heat transfer mechanism increases with increasing pressure but do not explain this claim at all. The predicted behavior from this effect is reproduced from their report in figure 3. The differences from the heat transfer limited model are shown to occur at low G. This mechanism was dismissed by them because their experiments led them into the pressure effects for high G and p_c.

The pressure dependence of radiative heat flux can be explained easily. The amount of radiation of the gas is dependent on the temperatures of the gas and the absorbing wall, as in equation(2.2), but the heat radiated must also be proportional to the number of radiators in the gas. As a result, if the gas pressure increases the number of radiators per unit

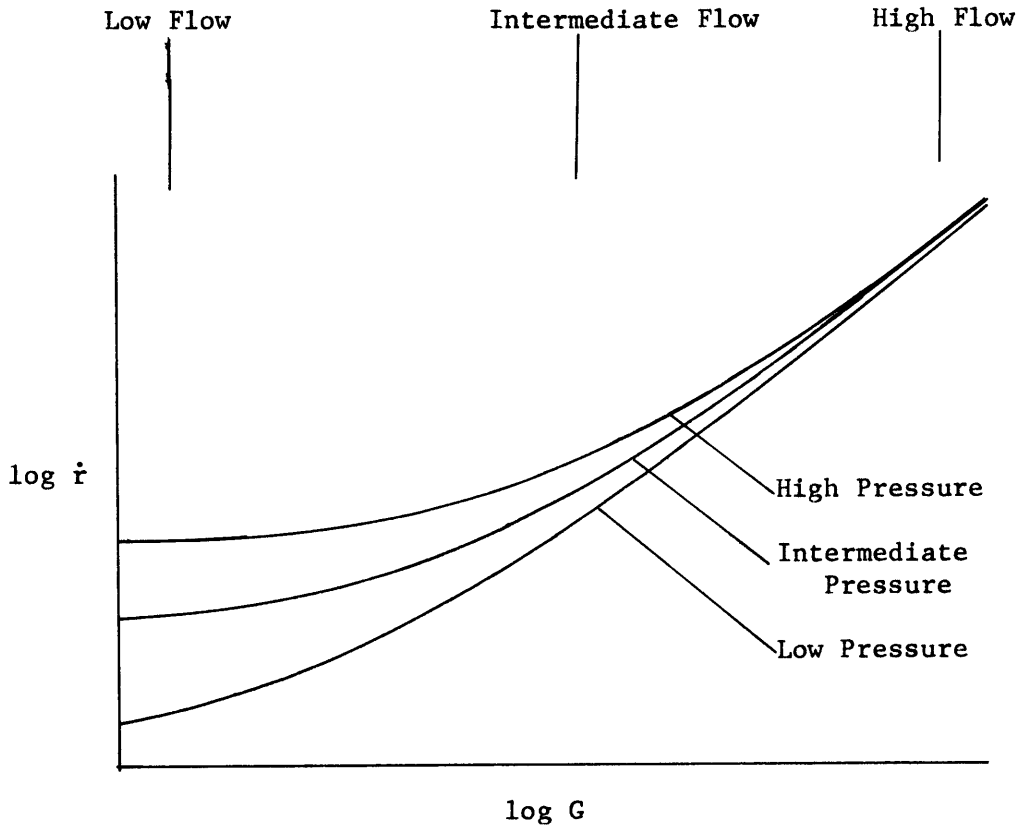

Figure 3 Radiation Effects

volume increases and the radiative heat flux must increase.

Smoot and Price then go on to consider and dismiss the assumptions that led to the model proposed later by Stickler and Kumar. The mechanisms dismissed are oxidizer reactions at the wall and fuel pyrolysis. Other pressure sensitive mechanisms considered were pressure dependence of equilibrium wall properties and gas phase kinetics, the last of these being chosen as "most likely". They do not appear to have convinced themselves however.

One parameter plays a very important role in all these models - the wall temperature. All of the models are very sensitive to changes in wall temperature. For the heat transfer limited model, T_w changes have a large effect on both $\dot{q}_r$ and Δh and thus have an important effect on the regression rate. The effect of T_w enters into the model of Stickler and Kumar by determining the average polymer chain length vaporizing and the kinetic rate, thus setting the fuel pyrolization rate.

A last point to make is the dependence of the velocity profile on the axial pressure gradient. The flame zome velocity seems to be very sensitive to small pressure gradients. If for some reason an adverse pressure gradient exists in the chamber for some period of time, boundary layer separation might occur, at which point all of these models become dubious. It is unclear whether the turbulent boundary layer combustion is unsteady to this extent in practical machines. The point at which turbulent boundary layers separate is ill defined, but (approximately) separation will usually occur.[1]

$$0.4 < \frac{\Delta p}{1/2\ \rho u^2} < 0.8 \qquad (2.16)$$

Here Δp is measured on a scale where viscosity is unimportant. In the

case of a hybrid combustion, there is an additional effect from blowing. This should cause separation for lower Δp than above since the wall mass addition is pushing the boundary layer away from the wall.

CHAPTER III

APPARATUS DESIGN AND CONSTRUCTION

3.1 Design

There are two basic, separate parts of the complete machine. These are the hybrid burner system and the vortex valve control system. The hybrid burner design and construction will be discussed first.

The parts of the small, plexiglas-oxygen hybrid rocket are shown in figure 4. The machine is divided into functional sections. The original purpose for the machine was a small, safe demonstration model rocket. It has very low thrust and uses clear plexiglas tubing as the fuel charge. The overall design was intended to get complete, steady state hybrid combustion within the chamber.

A flow rate of oxidizer into the chamber is first fixed by a pressure setting on a commercial regulator on a gas bottle, and a sonic orifice at the inlet to the combustion chamber. The orifice was sized at a diameter of 0.1 inch to give G values around 0.07 lb/in^2-sec at the available regulator settings; the "normal" hybrid operating regime. The sonic orifice also served to separate the combustion effects from the oxygen feed line.

The next purpose of the burner is to force the supersonic stream from the orifice to shock down and become a fairly uniform, low Mach number flow. This was accomplished by having a short section that grossly over-expanded the flow and induced strong shocks. The flow was then forced through a straightener. This consisted of a cylindrical block of metal, filling the channel, with two rows of holes on the periphery. These holes were made to have small diameter and a l/d ratio greater than 10, so

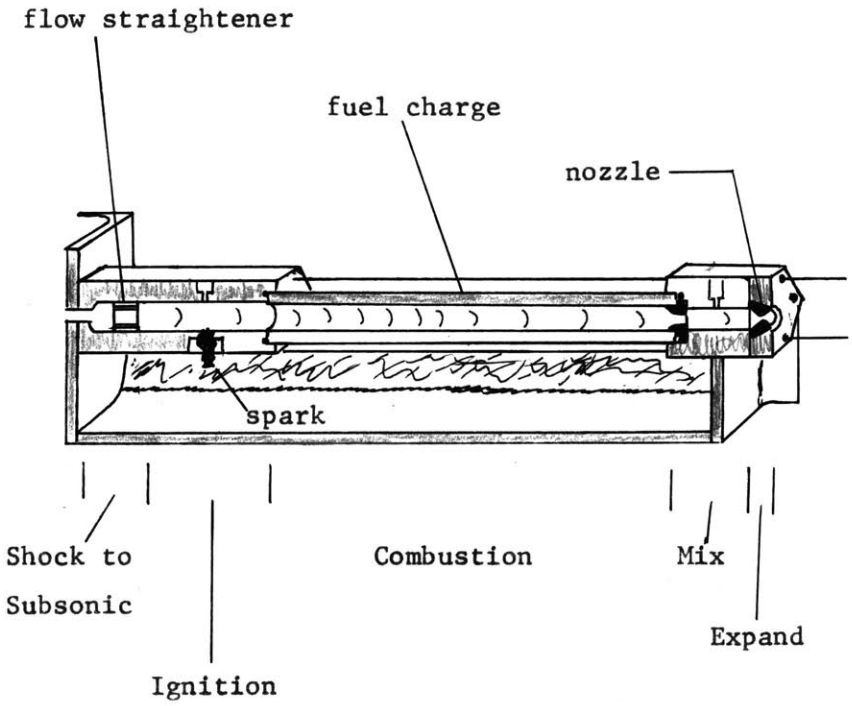

Figure 4 Experimental Hybrid Burner

that the boundary layers in each hole will fill it before the block ends, thereby removing a large part of the nonuniformities. The flow then expands abruptly to fill the channel again.

The ignition system follows the flow straightener. Methane was used here with a spark downstream to ignite the oxygen-methane mixture. The flow straightener was placed just far enough upstream of the methane inlet so that it was not exposed to the direct hot flow. The methane flow rate is set so that the mixture with oxygen is oxygen rich (to permit burning with plexiglas) and directed so that it reaches the spark rather than just washing downstream to create a detonable mixture.

The plexiglas fuel charge is what determined the overall sizing of the rocket. The length and inner diameter of the plexiglas tubing was set by basic fluid dynamical limitations, given the requirement of fairly small overall size. The length to diameter ratio was set at 10. For larger ratios, the boundary layers will fill the tube and remove the free stream of oxidizer. If the ratio is much less, the combustion behavior is then primarily determined by end effects. Furthermore, going below 1/2 inch inner diameter leads to difficulty in construction and measuring. This means that the average values used in hybrid models become more and more invalid. One inch channel diameter was thus settled upon as a practical, small rocket. The charges have a burning length of 10 inches.

The mixing section is designed to provide complete combustion of the fuel. This is necessary because a significant amount of fuel is transported unburned below the flame zone. At the end of the plexiglas charge, the flow is smoothly pinched inward by a graphite piece that ends abruptly, expanding the flow back to the 1 inch channel diameter. This expansion

causes flow separation and turbulent mixing, completely burning the remaining fuel. The combustion products are then dumped out of a sonic nozzle. The throat area of this nozzle determined the chamber pressure, set for about 100 psia maximum.

The vortex valve is a fluidic control device that can be viewed as a means of varying the virtual throat area of the exhaust nozzle. The basic physical layout of a vortex valve is shown in figure 5. The design parameters are the turndown radius, r_v/r_t and the cavity nondimensional thickness n/d_v.

The valve works by setting up a radial pressure gradient in the valve cavity. Since the circumferential pressure is the chamber pressure, and the nozzle sets the stagnation pressure directly behind it, by controlling the difference, the chamber pressure is controlled. For any element of mass entering the valve, the control flow gives it a tangential velocity. So the centrifugal force in the element must be balanced by the pressure for steady flow, and as the centrifugal force increases toward the center, the pressure decreases. The turndown radius, r_v/r_t should be 4 or 5 to get a significant pressure gradient across the cavity. The nondimensional thickness should also be about 1/5 or less so that there is very little axial velocity and the tangential control flow can be effective.

The valve used here has a $r_v/r_t \approx 5$ and $n/d_v \approx 1/5$. The flow had to be expanded from the 1 inch chamber channel and injected circumferentially by the graphite piece pictured in figures 10, 11, and 12. The exhaust area of the vortex valve nozzle was designed to place the chamber pressure in the region tested in the basic hybrid experiments, with the vortex valve operating. Theoretical valve effectiveness characteristics are such that

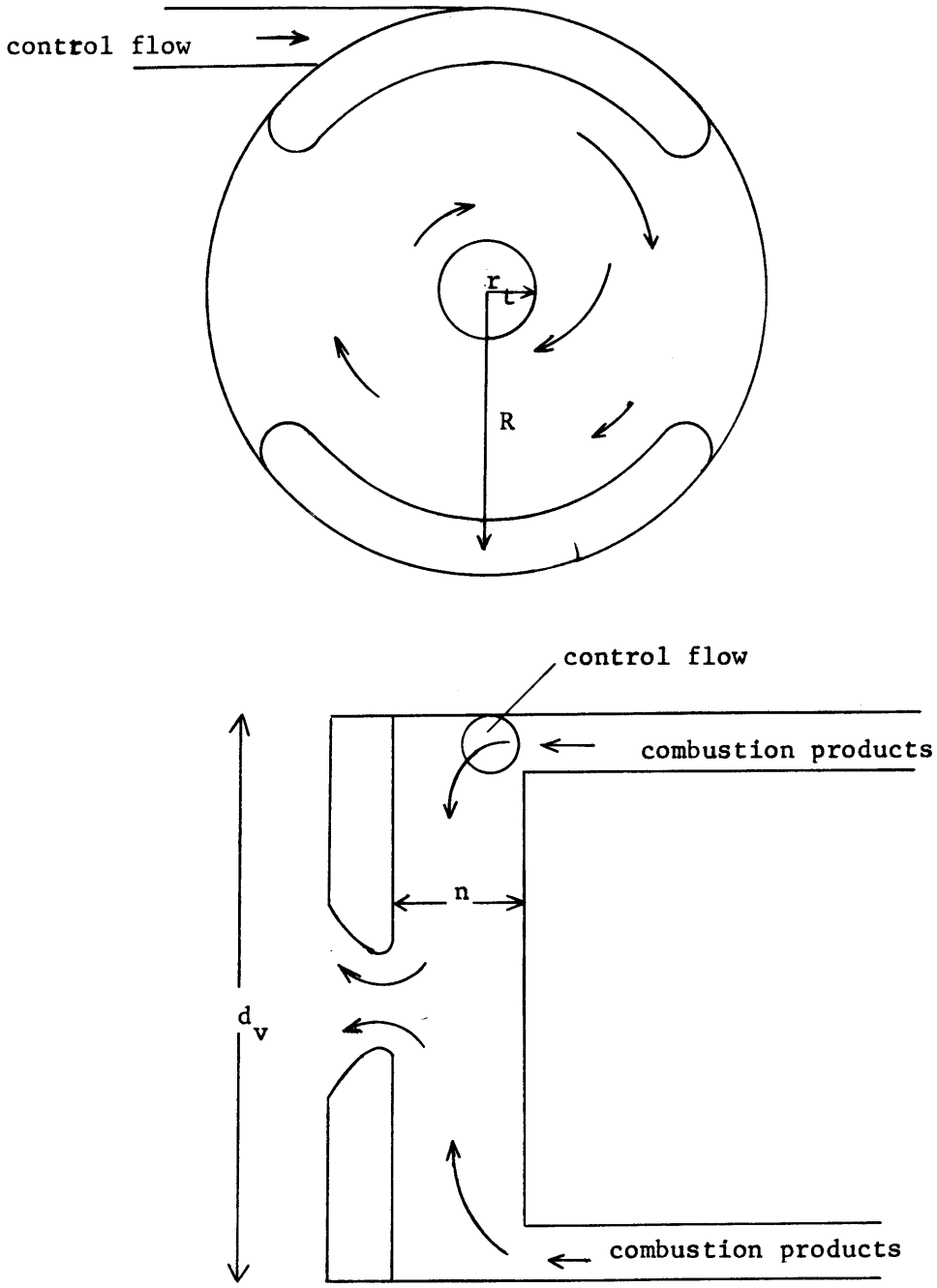

Figure 5 Vortex Valve Diagram

perturbations in the control flow should have the most effect for a steady tangential bias of close to 10% of the main flow.

All the above comments assume that the control and main flows are the same in all properties. Actually the only relevant property is c*, the characteristic velocity. For a sonic orifice:

$$\dot{m} = \frac{p_o A_t}{c^*} \tag{3.1}$$

$$c^* = \sqrt{\frac{RT}{\gamma M}} \left(\frac{\gamma + 1}{2}\right)^{\frac{\gamma + 1}{2(\gamma - 1)}} \tag{3.2}$$

So for the control flow we chose a gas whose T/M will be about the same as the combustion products. Since using a cold control flow gas is very advantageous, we seek a low T_{cf} and low M_{cf}. For plexiglas-oxygen, $T_c/M_c \simeq 60\text{-}70 \frac{\text{oK-gm-mole}}{\text{gm}}$ and since room temperature gas is easiest to supply, helium provides an excellent solution.

A device was next designed to modulate the control flow into the valve. First a fluidic oscillator was tried, using a fluid capacitance attached to the vortex valve with opposing tangential inlets. The device is sketched in figure 6. It used the capacitance as a resonant volume with an oscillating direction of tangential flow in the valve. The frequency was to be changed by varying the capacitance volume. This device was built, but was found impractical because chamber pressure oscillations were not far different from noise.

The method actually used is sketched in figure 7. It employs a simple rotating ball valve arrangement that pulses part of the control flow at a frequency set by the speed at which the shaft operates. This provides a pulsed flow on top of a steady bias flow which will drive chamber

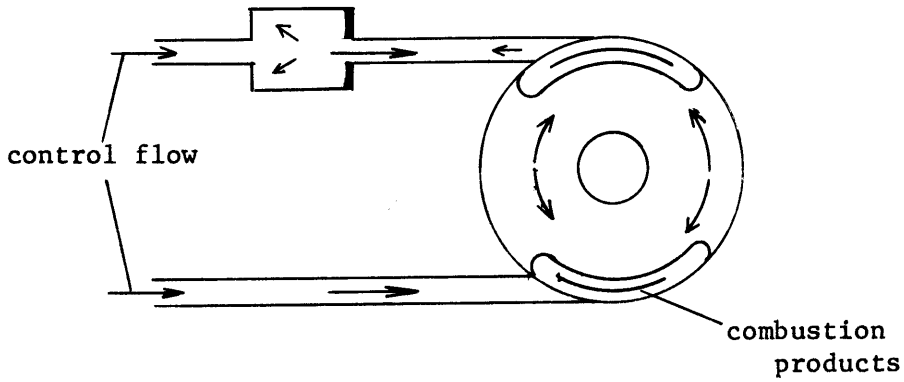

Figure 6 Fluidic Control Flow Modulator

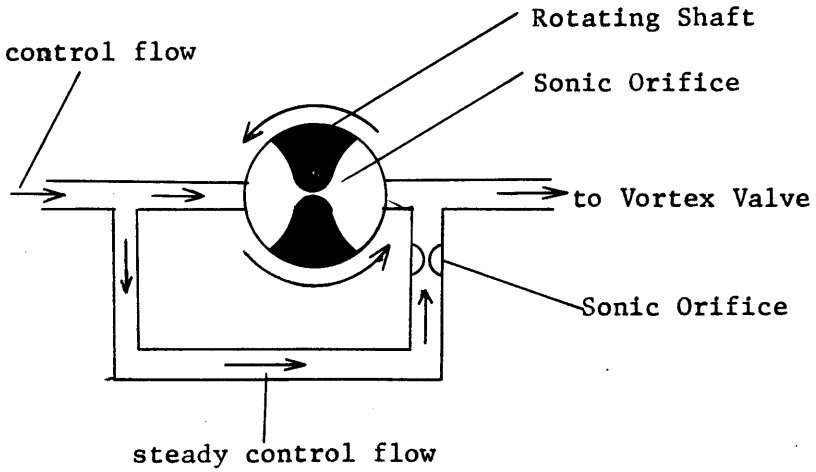

Figure 7 Mechanical Control Flow Modulator

pressure oscillations.

3.2 Construction

The complete machine, including the vortex valve and its driver, are shown in figure 8 without connecting equipment. The rocket and valve were designed and built with a conscious effort toward simplicity, since I provided the labor. The base is made out of aluminum as is the flow control block pictured in the upper left hand corner. Aluminum was used where temperatures permitted, but even the flow straightener had to be steel after the failure of some aluminum honeycomb. The caps in the picture are for pressure transducer connections, while the uncapped fitting is the methane inlet. The methane is injected tangentially as an attempt at better ignition characteristics. No careful testing was done on this, primarily because there were no real ignition problems with pure oxygen. (There are severe problems for air.)

The first sonic orifice is just downstream of the ball valve, with a fitting between it and the ignition block. There is also a sonic orifice in the methane inlet but in this particular case the gas line was so long that the main function of the orifice was to isolate the line from the chamber pressure.

It is not clear from the picture, but the only rigid connection between the base and the rocket body is six bolts around the oxygen inlet. The downstream end rests freely on the support and the different pieces are held together axially by the three steel rods screwed into the ignition block with nuts on the downstream end. The ignition block has been described before except for the spark plug used for the back motors. The spark itself only protrudes into the flow about 1/8 inch.

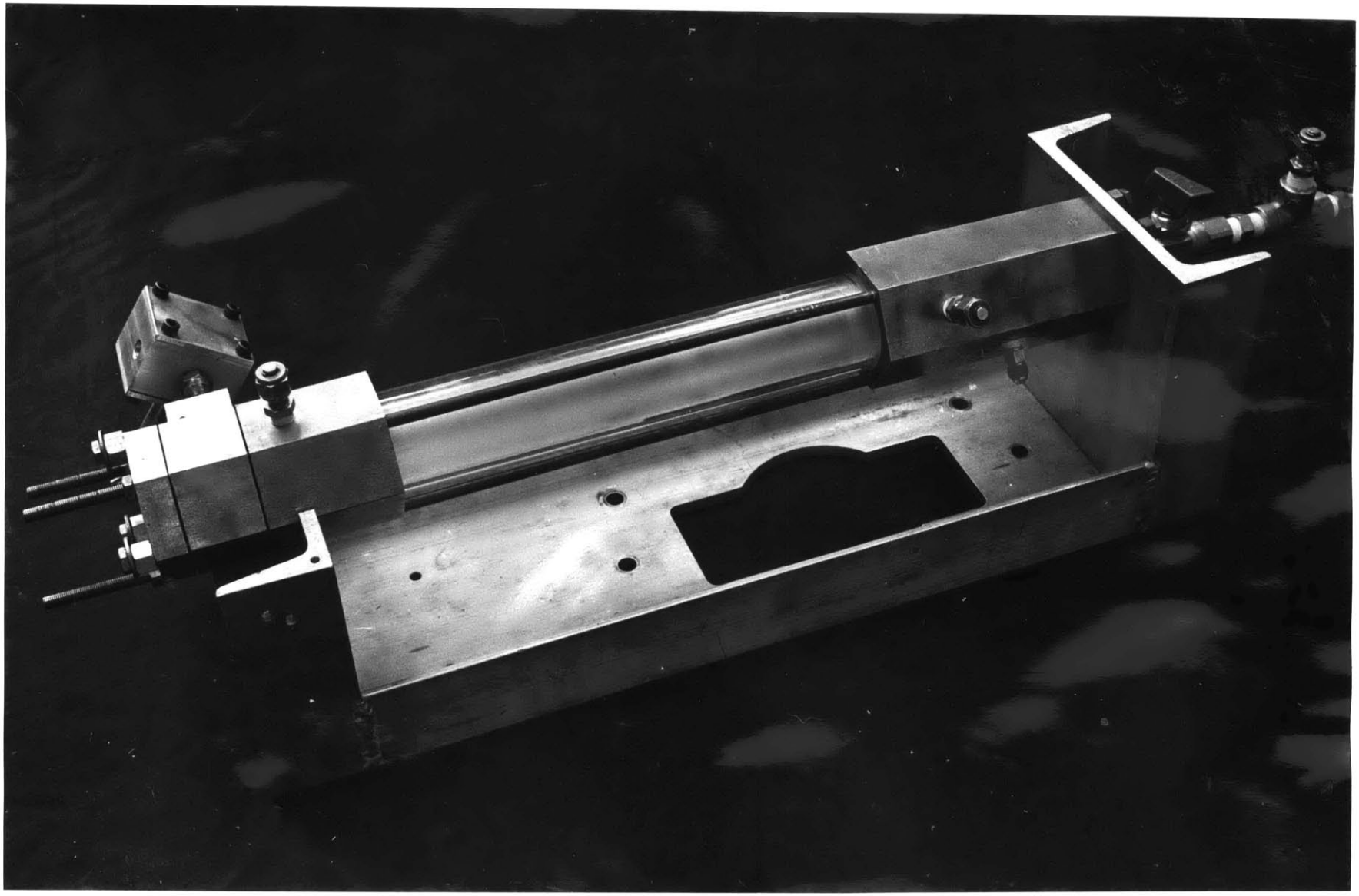

Figure 8 Stripped down oscillation test rocket

The plexiglas tubing used for fuel is commercially cast into tubes of maximum thickness 1/4 inch. Two concentric tubes are actually shown in the picture. The outer tube serves as a pressure vessel (with a large safety factor) and is sealed on either end by silicone rubber O-rings. The inner tube is the fuel charge and is burned to the extent that the outer tube is reusable.

The next piece downstream is the mixing block. The upstream end is shown in figure 9. Here we see the O-ring on the outside, recessed into the block, and the graphite mixing piece at the center. Graphite was used because it sees the full high temperature flow, which would melt even steel. Also note that the back side of the mixing piece is flat with no rounded edges.

For the basic hybrid tests, the mixing block would then be followed by a graphite nozzle. In the final phase of testing the next piece was the vortex valve shown in figures 10, 11, and 12. Figure 9 shows the front of the valve assembly. The center is again graphite to withstand the direct bombardment of hot flow. Setting up the holes as shown, as opposed to equally spaced was merely a quirk of machining. The other end of the valve (figures 11 and 12) has a cavity of diameter 1 1/2 inches with a nozzle diameter of 0.34 inches.

In figure 11, the tangential control flow hole is visible toward the top, the bright spot being the stainless steel tube for control flow. This tube is inserted into the graphite and silver soldered to the fitting. Two tangential holes are evidenced by the screw blocking the unnecessary one. Asymmetry is provided to the hex stock by two pieces of steel brazed on merely to get enough steel to screw the fittings into. The pressure

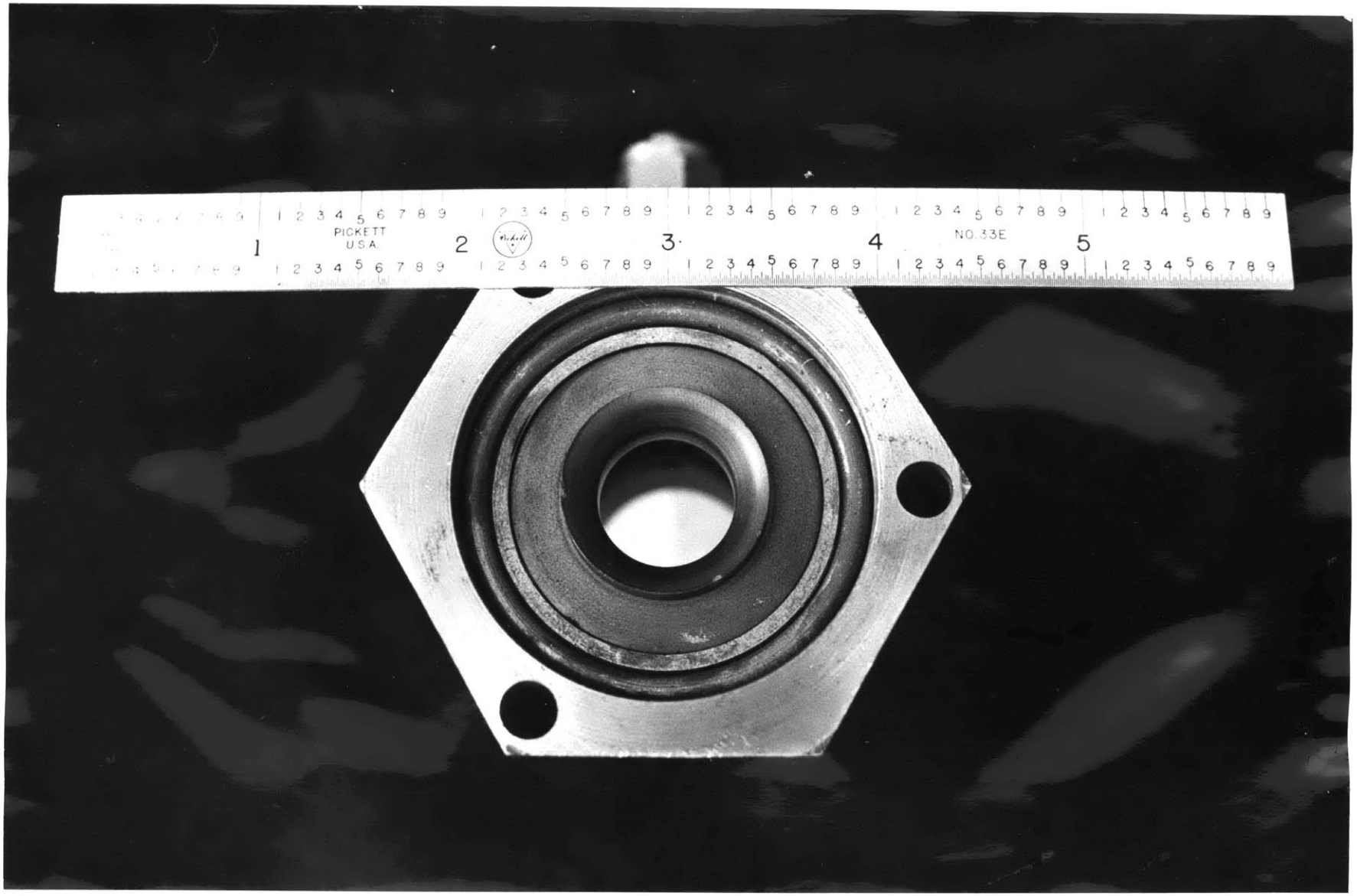

Figure 9 Mixing Block

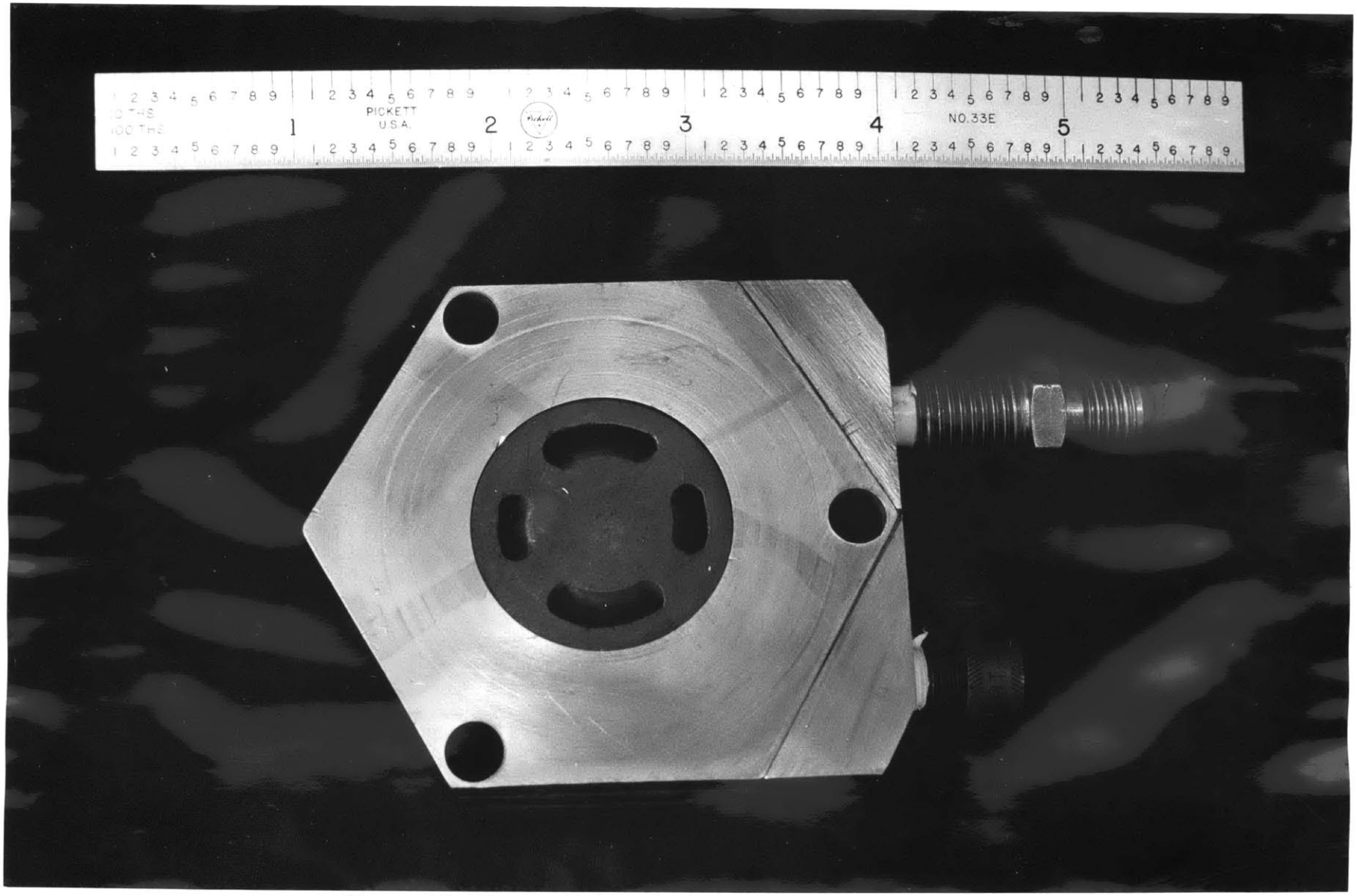

Figure 10 Vortex Valve Block - upstream view

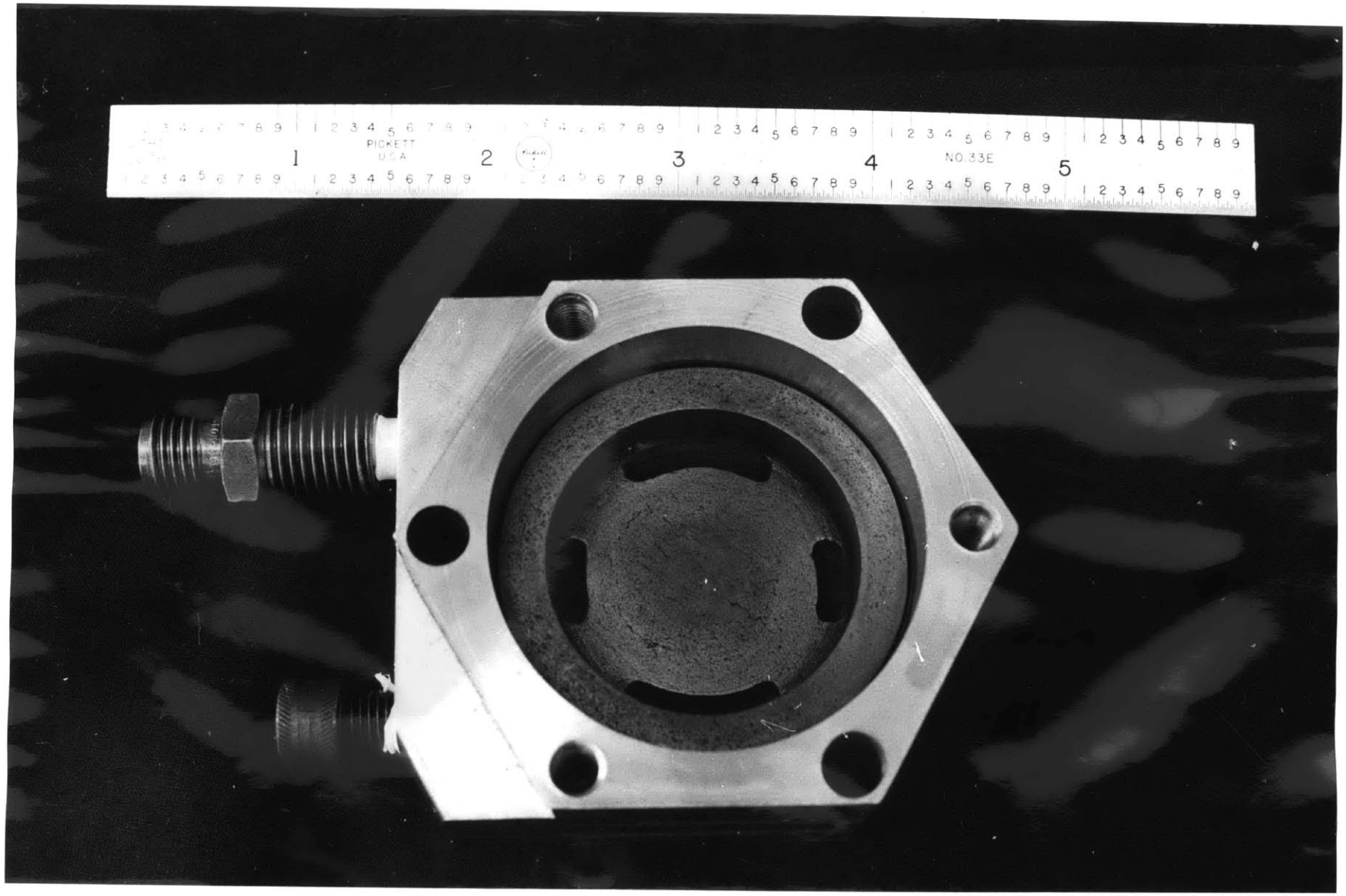

Figure 11 Vortex Valve Block - downstream view

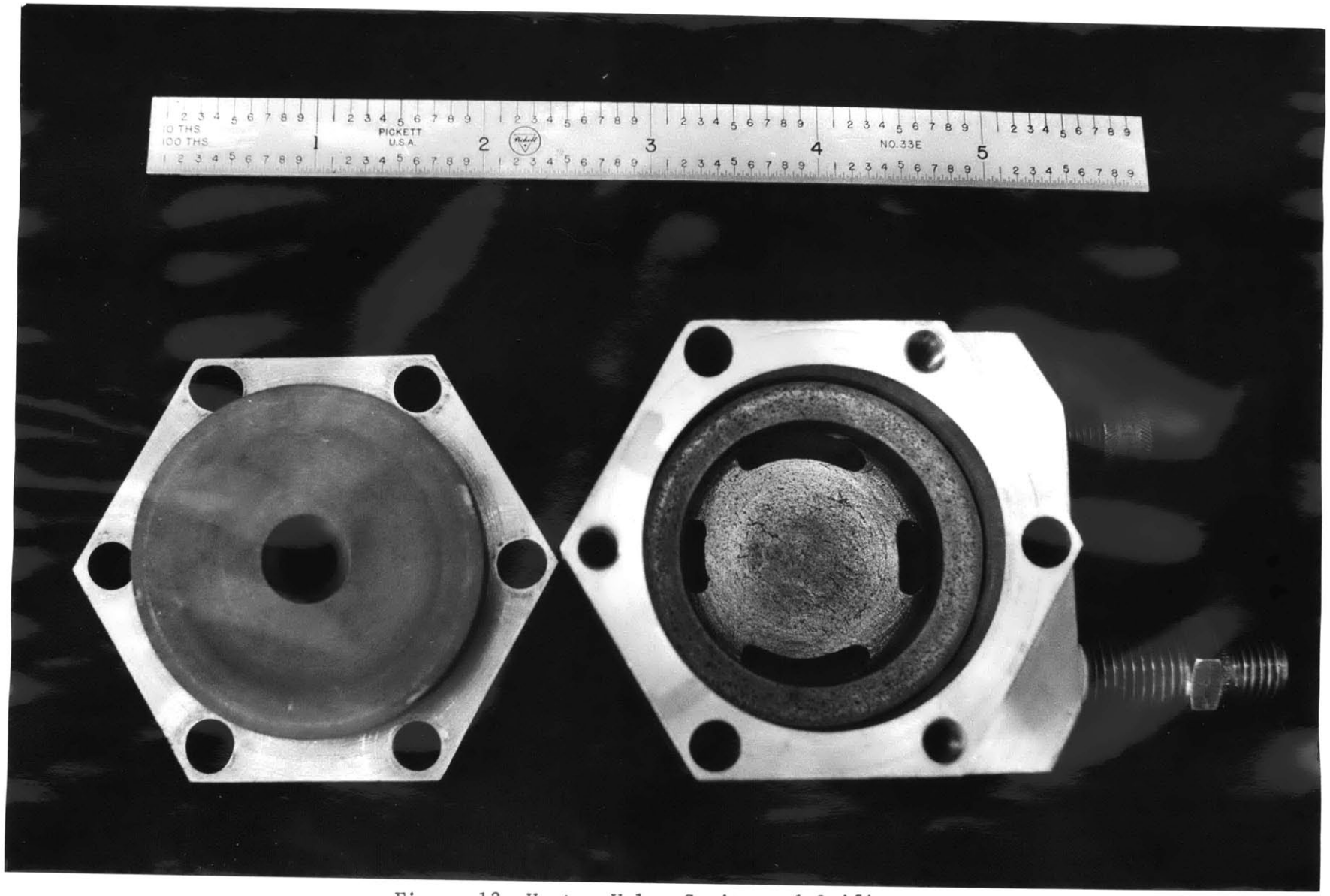

Figure 12 Vortex Valve Cavity and Orifice

seal on the vortex cavity was from graphite to graphite contact, while the whole assembly was sealed to the mixing block by an O-ring in the end of the mixing block.

The mechanical control flow regulator is seen hanging onto the vortex valve in figure 8. The device is made out of an aluminum block with a stainless steel shaft for a flywheel effect in maintaining constant speed against variable resistance. Ball bearings on either end of the block hold the shaft and are held on in turn by aluminum plates, seen screwed on in figure 8. Sonic orifices in the shaft and block are screws set in (that can be changed) with the orifices in them. Pressure seals on the shaft were managed by a gasket on the closed end and an accepted leak around the shaft to the motor.

Apparatus associated with the rocket and vortex valve is shown in figure 13 and is self explanatory. The strip chart recorder takes the voltage signals from the pressure transducers, converts them to light beam traces with galvanometers, and then records the beam traces on light sensitive paper. A constant paper speed gives a pressure versus time record of a run.

Gas control was all performed by hand on the ball valves shown except that the oscillating flow line valve was always left open. Standard gas bottles and pressure regulators were used. Variable shaft speed was achieved with a variable voltage source supplying the motor, which was a D.C. generator in reverse.

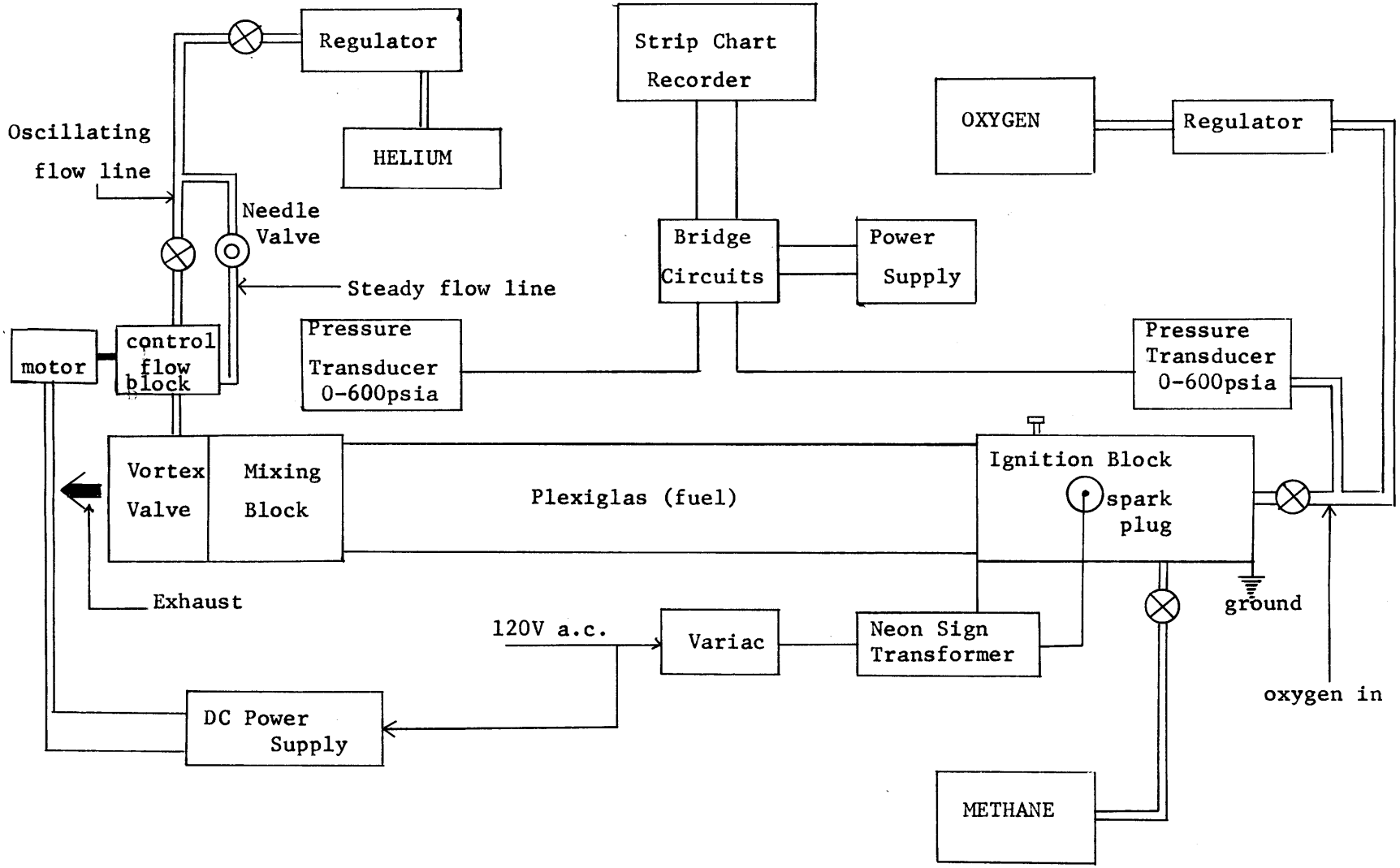

Figure 13 Peripheral Apparatus

CHAPTER IV

EXPERIMENTAL PROCEDURE

Once the apparatus was actually constructed, the main experimental procedure was to make sure everything was connected and tight. For each test of the hybrid rocket without the vortex valve, one new inner charge of plexiglas was used and then the end of the machine was dismantled to remove it. The outside of the burned tube was coated with silicone grease so that it would not bond with the larger tube as happened in earlier tests. Also, runs 1 - 9 and 10 (see tables 1-2) destroyed the graphite nozzles in varying degrees due to the high temperature and oxidizing atmosphere (about 10 nozzles were made eventually). The graphite mixing piece was subjected to the same temperature, but it was in a fuel rich atmosphere. It got red hot but suffered no erosive damage. It was necessary, however, to coat the contact surface between the plexiglas and graphite, again to prevent bonding.

A very major problem with graphite nozzle erosion was solved, allowing completion of the vortex valve testing. Before and after cases are shown in figure 14. The method was to coat the graphite with commercial silicone grease. This was not only effective but simple. It was tried as a pure guess and it worked. The mechanism involved is not absolutely certain. There two main possibilities however - there was either a reaction to give SiO_2 or SiC. The former might appear more likely because of the oxidative attack on the graphite, but the melting point of SiO_2 is 2000°K which is just about at or a little below the predicted gas temperature in the flow. On the other hand SiC has a melting point at 2700°K. After a

Figure 14 Nozzles - Unprotected and Coated

run, the nozzles had a thin, flaky whitish-grey coating which would indicate SiO_2 rather than a darker crystalline coating that comes from SiC. The conclusion is that the coating is indeed SiO_2. The fact that it stood up to the high temperatures can be attributed to the excellent heat conductivity of graphite which would place the wall temperature at perhaps 1700°K - below the melting point of SiO_2 and above the temperature at which the graphite oxidation becomes important (~1500°K).

The actual time sequence of functions during a run was set up to minimize problems and maximize data. The sequence is: 1) Spark on, 2) Recorder on, 3) Oxygen on, 4) Methane on, 5) Methane off, 6) Helium on, 7) Helium off, 8) Oxygen off, 9) Recorder and spark off. This is of course for the complete apparatus with the vortex valve. Each regulator was set before each run and the vortex valve touched up with silicone grease. This last act was a precautionary measure that was relaxed with time with no ill effects observed. Also, during vortex valve experiments, the motor was turned on before the test sequence and turned off after everything else, so for the hot flow data the oscillator box shaft is always rotating.

The crux of any good set of experiments is not the busy work that must always be done, but the interaction between data and experiment. Often one set of experiments determines the direction of future tests. Rarely are they independent.

The experiments done here were in two basic parts - hybrid combustion tests and vortex valve combustion pressure oscillation tests.

The first of these was intended to study two things for the purposes of this thesis. One is to get data on the basic hybrid process, and that process in this particular machine. Conditions were varied to cover the

entire range of conditions expected to be encountered when using the vortex valve. A side purpose of this data was to see how well it corresponded to the far from accepted theory on the region of operation. It was expected that the tests would be partially in one of the previously mentioned pressure sensitive regimes. As time and nozzles passed, another side issue became graphite protection. Ignition was no problem using pure oxygen.

The basic determining parameters are G and the chamber pressure. G was simply varied by changing the oxygen feed pressure and thus the mass flow rate through the sonic orifice. The oxygen regulator pressure was varied in intervals of 50 psi from 200 psig to 400 psig through a 0.1 inch diameter orifice. This variation was performed twice, each set with nominally one exhaust nozzle area. The mass flow combustion temperature and exit area would then set the chamber pressure. However the pressure was incremented pretty much randomly from 50 to 100 psia as the oxygen feed pressure was changed. Thus turned out to be fortunate since it enabled somewhat better correlation of the chamber pressure with the burning rate $\dot{r}$.

For these hybrid tests the pertinent data obtained was a burn time, oxygen feed pressure, average chamber pressure, fuel mass loss and nozzle throat diameter. The first three came from the strip chart traces and the last two from direct measurements before and after.

The second objective of the hybrid tests was to study the pressure instabilities that appear. They were just observed in the first 11 runs of the basic testing. Then some tests were done, based on the 11 runs, to see what was causing the instabilities. There were only two of these.

One was to find out if the instabilities were slosh mode or bulk mode; by examining the pressure variation phase difference. This was done by putting a transducer on each end of the chamber and comparing the nearly superimposed traces on the strip chart. The other test was to remove the protruding part of the mixing piece and see the effects of incomplete combustion on the pressure oscillations.

Next came the tests with the vortex valve. Initially the tests were made in the order of increasing complexity. Tests were begun with control flow and no other flow. The chamber pressure was found to increase with increasing steady control flow and oscillate when the unsteady flow was turned on. Then the effects of varying the motor speed were observed under the same conditions. After this, the same tests were repeated with oxygen flow and no combustion. Once this had been done, and the mechanism was found to work, consideration had to be made on how to operate the vortex valve during combustion. So, with the motor on throughout, we found out how long it took the chamber pressure oscillations to become steady after the control flow line was pressurized by turning a ball valve. This being very short, it was possible to go on to combustion control with the controlling sequence previously mentioned.

Going gradually to more stringent conditions, different motor speeds were used with combustion and no steady control flow. This with the recognition that the pulsed control flow is most effective around a definite steady flow bias of about 10% of the main flow. The same motor variation was then done with the steady flow on full. Since the inherent hybrid pressure oscillations were found to be larger than those induced, lesser amounts of steady flow were dispensed with. This effect served to disguise

the induced oscillations also. Having finished these, we attempted to drive the instabilities at resonance. Again, fortunately, the available motor speeds allowed us to bracket the instability frequencies (i.e., lower to higher).

Polishing up the vortex valve experiments, the pressure was again measured at both ends of the chamber. This enabled us to see if there was any phase difference in the pressure variation between the two ends, and any large axial pressure gradient. As a final set, recordings were taken of cold flow oscillations with all control flow on and for different motor speeds. The result lead to a comparison between cold and hot flow effects of the vortex valve for the same flow rate of oxygen.

For each hot flow test, before and after a run, the control flow was turned on and a recording was made of the pressure variation. The motor voltage was not touched until these and the hot run were recorded. The purpose of this was to get an accurate knowledge of the frequency of the oscillation because the motor speed was changed by the gas flow resistance.

That is what the major tests and motivations were.

CHAPTER V

CALCULATIONS AND RESULTS

5.1 Basic Hybrid Tests

There are five numbers that resulted from each test of the hybrid rocket. These are the fuel mass loss, the burn time, the oxygen feed pressure, the average chamber pressure (taken on the downstream end), and the nozzle throat diameter. The values for these are listed for each of the twelve runs in Table I.

Some of these numbers represent averages. The throat diameters were measured before and after and then averaged. This occurred for all the runs except 11 and 12, which used the coating discovered as a result of Run 10. Run 10 took place at the highest chamber pressure and flow rate expected, with an uncoated nozzle. What happened is shown in figure 14 with the coated nozzle that was subsequently used for Run 11 to successfully complete the test sequence. Appendix A gives the extreme variations in throat diameter and chamber pressure for each run. Also note that the set oxygen regulator pressure went from 200 psig to 400 psig in increments of 50 psia; p_{ox} resulted from that, line losses, and bottle pressure.

Additional useful data is the oxygen sonic orifice diameter: 0.100 inches, chamber diameter; 1 inch, burning length: 10.0 inches, and a chamber length of 16.5 inches. The mechanical drawings in Appendix B will provide any exact measurements necessary. The length of the plexiglas tubing was 10.2 inches to account for the 0.2 inch nose of the mixing section.

Much information is contained in the raw data given. Certainly not all of it is used here.

Run	M_L	t_b	P_{ox}	$\overline{P}_c$	d_t
1	34.2	11.0	160	49	.34
2	57.7	15.7	189	54	.36
3	51.5	12.5	228	70	.35
4	54.8	11.8	266	83	.34
5	66.0	12.4	297	89	.36
6	39.9	13.0	144	58	.31
7	53.4	14.5	183	67	.32
8	49.4	11.5	229	86	.31
9	44.1	9.8	263	97	.307
10	66.8	13.2	292	85	.36
11	45.5	9.5	279	105	.305
12	36.2	10.7	198	49	.382
Units	grams	seconds	psia	psia	inches

Table 1 Raw Data

The first result is the average mass flow of fuel, $\dot{m}_f$.

$$\dot{m}_f = \frac{M_L}{t_b} \tag{5.1}$$

Then oxygen mass flow:

$$\dot{m}_{ox} = \frac{p_{ox} A_{tox}}{C^*_{ox}} \tag{5.2}$$

$$\text{or,} \quad \dot{w}_{ox} = \frac{p_{ox} A_{tox}}{C^*_{ox}} g$$

Here C^*_{ox} [see equation (3.2)] is gotten using M = 32, T = 300°K, γ = 1.4 which gives C^*_{ox} = 1340 ft/sec. Also G and $\bar{\dot{r}}$ can be calculated

$$G_{ox} = \frac{\dot{m}_{ox}}{A_c} \tag{5.3}$$

$$G_f = \frac{\dot{m}_f}{2A_c}$$

using the fact that the boundary layer will grow approximately linearly down the charge and averaging.

$$G_{tot} = G_f + G_{ox} \tag{5.4}$$

This number is useful because the regression rate depends on the total G at any point down the duct for the heat transfer limited model.

The burning rate can be calculated as a first approximation from:

$$\rho_f A_b \bar{\dot{r}} = \dot{m}_f \tag{5.5}$$

Where $\rho_f = 1.19$ g/cm^3 for polymethylmethacrylate - plexiglas. As a better approximation, the changing burning area can be included by another average.

$$\dot{m}_f = \rho_f \bar{\dot{r}} \pi L (d + \dot{r} t_b) \tag{5.6}$$

Calculated values for the above parameters are presented in Table 2 including an overall stoichiometry, which is quite different from the flame stoichiometry. The value of $\bar{\dot{r}}$ given is the corrected value, iterated from equation (5.5) in (5.6) for accurate computation. Again, values are both time and length averaged.

B, also presented in Table 2, is another revealing parameter for correlation with mass addition. Since the B values observed here were on the border of the two regimes of equation (2.7) and (2.8) both values were calculated. All but runs 1, 6, and 7, B is thought to be more accurately given by (2.7) but for these runs it is not clear whether (2.8) should be used or some appropriate average.

The search for correlations in the data in Table 2 is begun with a plot of $\bar{\dot{r}}$ versus G as suggested by the heat transfer limited model. The difference in point notations indicates that fuel charges were obtained from different orders of plexiglas. The fabrication of the tubes can change the burning rate behavior significantly with a slight change of cure catalyst in the plexiglas. The graphical results given in figure (15) are partially in agreement with the predicted $\bar{\dot{r}} \propto G^{.8}$. The differences occur at the lower values of G and are seen to <u>consistently</u> grow with increasing pressure dependent mechanism shown in figure 3. Another factor which points to this as the correct mechanism is that the B values calculated are in agreement with those predicted for the radiation effects to be significant when

Run	$\dot{w}_{ox}$	G_{ox}	$\dot{w}_f$	G_f	G_{tot}	$\bar{\dot{r}}$	$\frac{O}{F} = \frac{\dot{m}_{ox}}{\dot{m}_f}$	$\bar{P}_c$	B(Eq2.7)	B(Eq2.8)
1	3.02	3.85	.674	.436	4.29	4.80	4.42	49	4.95	5.5
2	3.57	4.55	.809	.515	5.06	5.50	4.42	54	4.64	4.9
3	4.30	5.48	.906	.578	6.06	6.23	4.75	70	4.10	3.86
4	5.02	6.40	1.02	.651	7.05	7.00	4.91	83	3.77	3.13
5	5.71	7.29	1.17	.745	8.04	7.90	4.88	89	3.60	3.02
6	2.72	4.40	.675	.430	3.89	4.70	4.03	58	5.95	8.2
7	3.46	5.51	.809	.515	4.91	5.56	4.28	67	5.10	5.95
8	4.33	6.34	.944	.600	6.11	6.50	4.59	86	4.39	4.32
9	4.97	6.72	.992	.631	6.97	6.90	5.01	97	3.75	3.10
10	5.52	7.04	1.11	.707	7.75	7.49	4.97	85	3.57	2.81
11	5.27	6.72	1.05	.669	7.39	7.29	5.02	105	3.70	3.02
12	3.74	4.76	.744	.474	5.23	5.16	5.04	49	3.70	3.02
factor	$x10^{-2}$	$x10^{-2}$	$x10^{-2}$	$x10^{-2}$	$x10^{-2}$	$x10^{-3}$	-	-	-	-
units	lb/sec	lb/in^2sec	lb/sec	lb/in^2sec	lb/in^2sec	in/sec	-	psia	-	-

Table 2 Calculated Hybrid Parameters

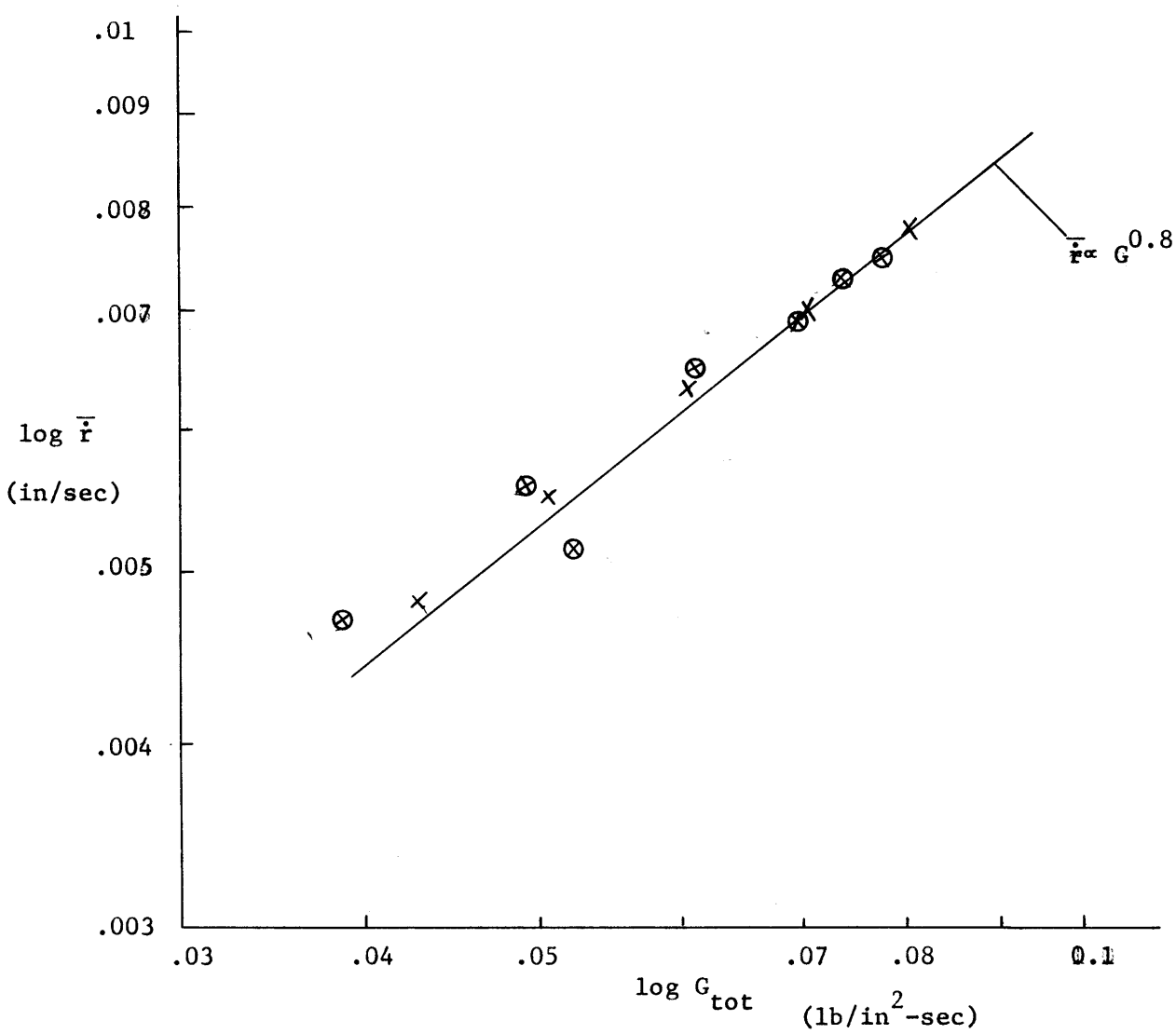

Figure 15 $\dot{\bar{r}}$ vs G Plot

changes from $\bar{\dot{r}} \propto G^{0.8}$ are seen to occur. This experimental behavior has been recorded before.[6,2] Maxman et al. explained it as an effect of melting, but here the wall temperatures are too high for this effect to be significant. The conclusion is that the heat transfer limited theory, coupled with radiation effects provide explanation of the observed regression rate behavior.

The one point in figure 15 that does not fit in with the above explanation is the data taken without the mixing piece. The lower burning rate can easily be attributed to the loss in enthalpy release due to the existence of a significant amount of unburned fuel.

It appears that no other significant correlations can be found. It is tempting to assign some correlation with the regression rate and the chamber pressure, but the change in chamber pressure is primarily due to the change in G through the constant area nozzle. The nozzle erosion gives enough variation in the chamber pressure increments that the correlations directly with the chamber pressure are seen to be unlikely.

The pressure versus time recording of Run 6 is shown in figures 16, 17, and 18, as a trace of the strip chart record. It is a typical run. There are some other miscellaneous, but possibly important observations made about the runs. One point to note is that the boundary layers did not fill the tube. If they had, the overall oxygen to fuel mixture ratio would have been much closer to the stoichiometric value of $O/F \simeq 2$. Also, after each run, the degraded plexiglas was observed to have non-uniform, finely speckled, dark grey bands on each end with a clean surface at the middle. These regions measured 2 to 3 inches from the tube end to the end of the region closest to the other end. The upstream region was always a fraction of an inch longer. No satisfactory explanation has been found

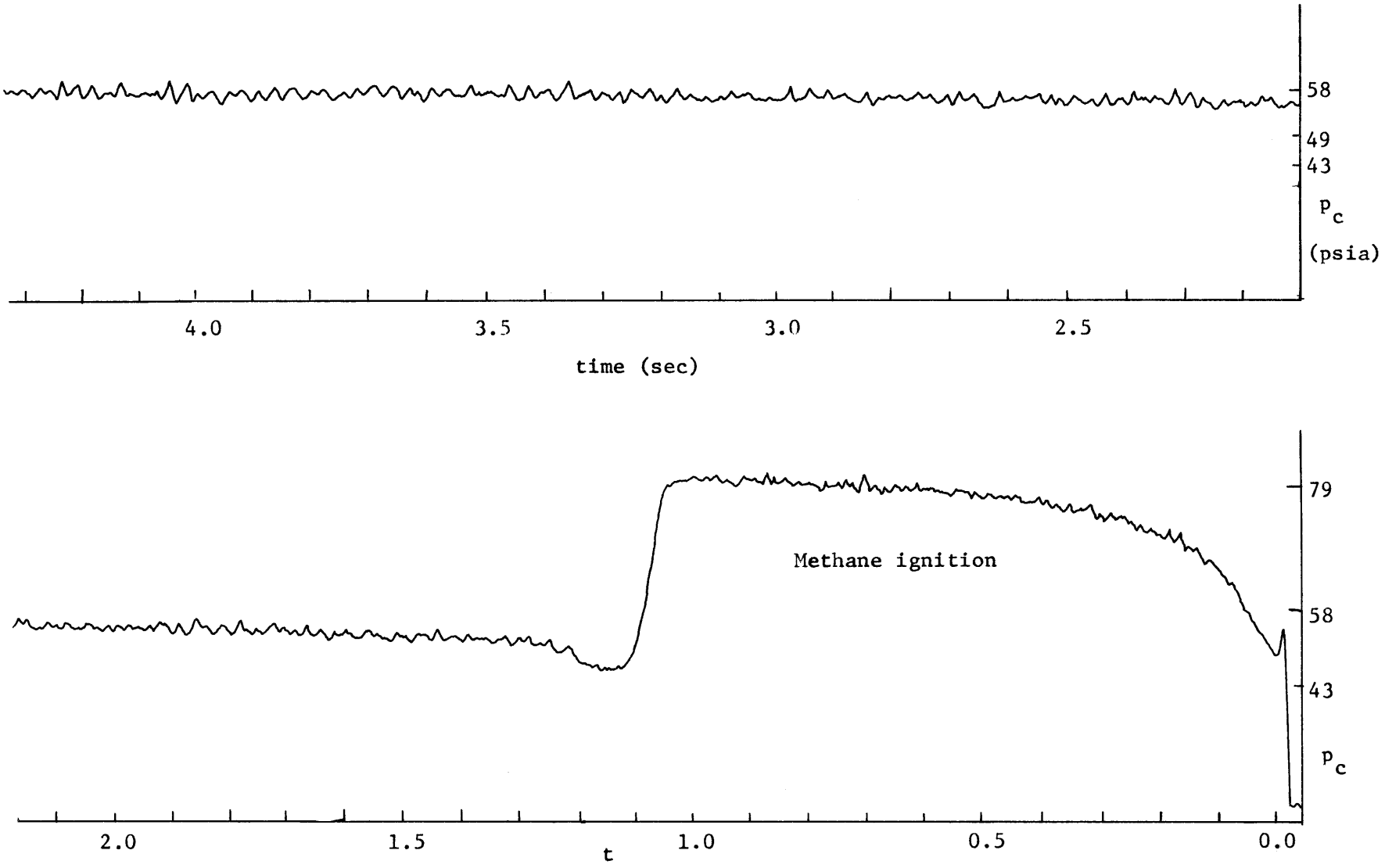

Figure 16 Experimental combustion test - Run 6

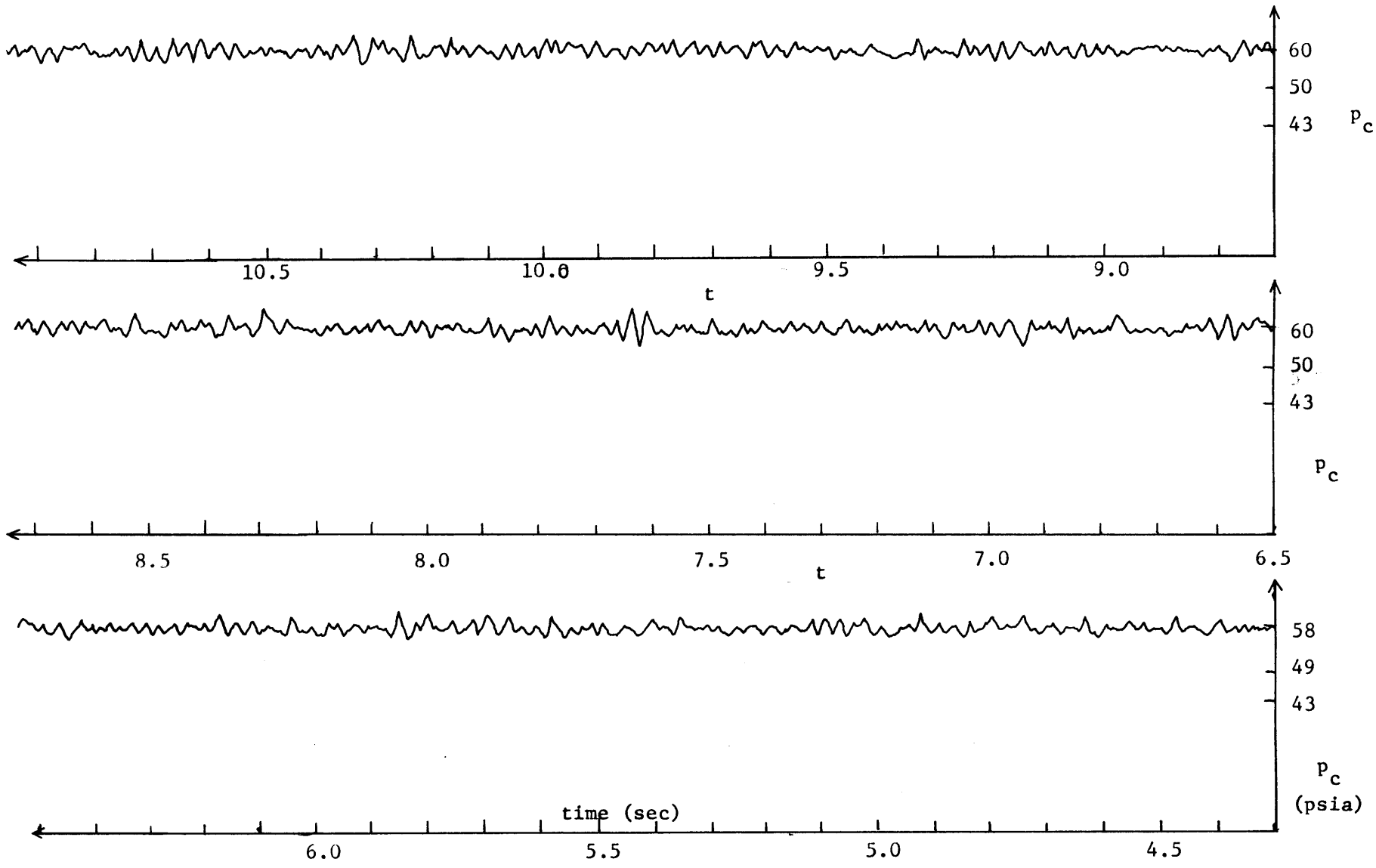

Figure 17 Run 6 (continued)

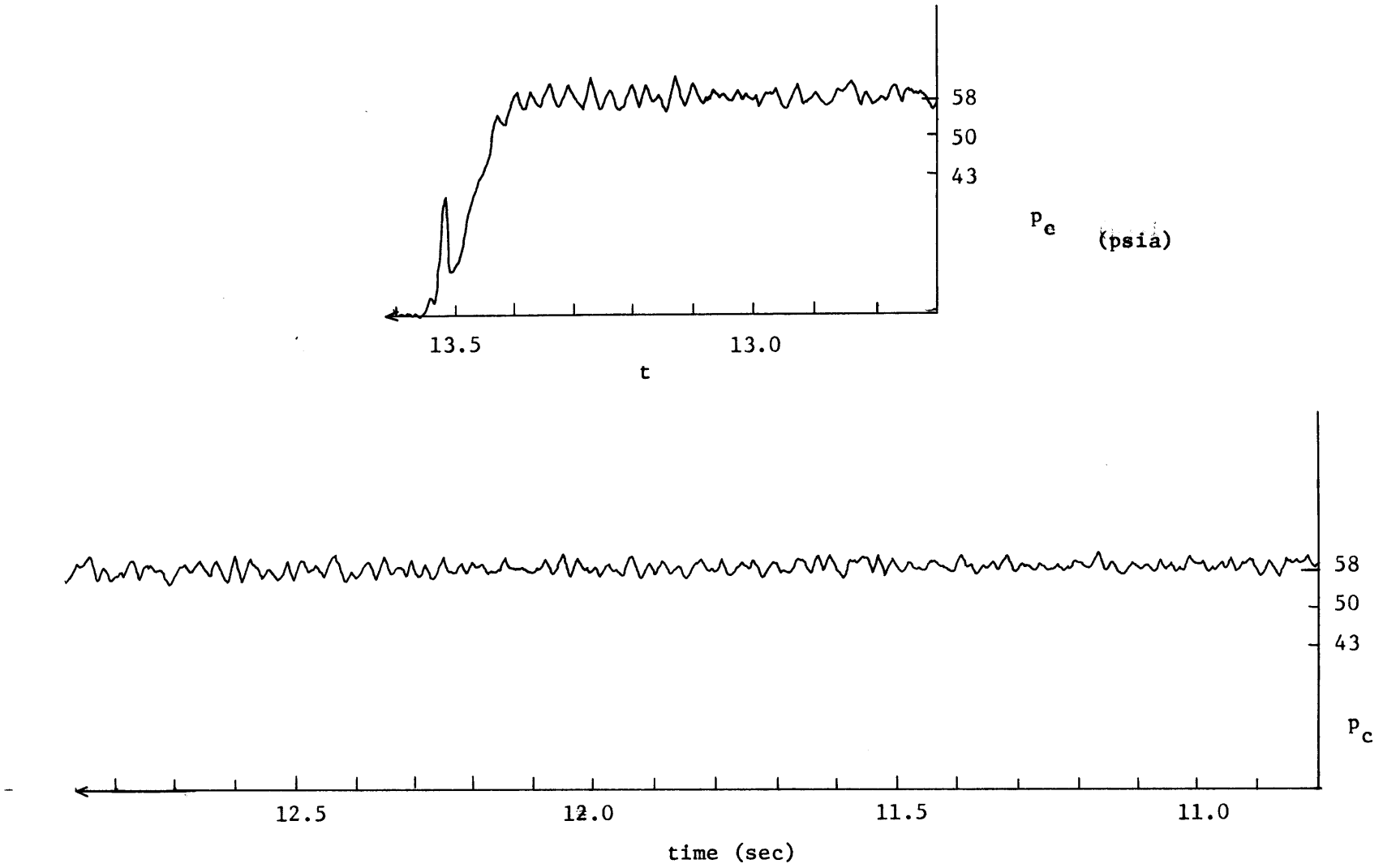

Figure 18 Run 6 (continued)

for the existence of these regions.

5.2 Instability Data

Figure 19 shows a plot of the maximum peak-to-peak ($\hat{p}$-$\check{p}$) pressure variation versus chamber pressure. It indicates that the peak-to-peak pressure amplitude is a constant fraction of the chamber pressure - somewhere between 7 to 10%. The uncertainty comes from the randomness of the oscillations and errors in both p_c and p-p measurements. Thus, the first point to recognize is that the oscillation amplitude is primarily a function of chamber pressure and not G. This became obvious in Run 10, where the chamber pressure dropped by about 2/3 as did the oscillation amplitude, while G remained constant.

An approximate frequency of 40 cycles per second can be seen in Run 6. This frequency was the same in all the runs to the extent that it can be called a given frequency.

There were two tests at this point to try to pin down the mechanism for the oscillations. A simultaneous recording of the pressure at both ends eliminated the possibility of a low frequency sloshing mode and indicated that there was a significant favorable pressure gradient (5-20 psia) across the fuel charge (~72 psia upstream, ~60 psia downstream in the one phase test). The results of removing the mixing piece are shown in figure 20. The conclusion from this is that the mixing is a very important part of the mechanism causing the instability. At the very least it acts as an amplifier to other random disturbances.

5.3 Vortex Valve Data

The tests with the vortex valve were performed always at an oxygen regulator pressure of 250 psig and a helium pressure of 185 psig. The same

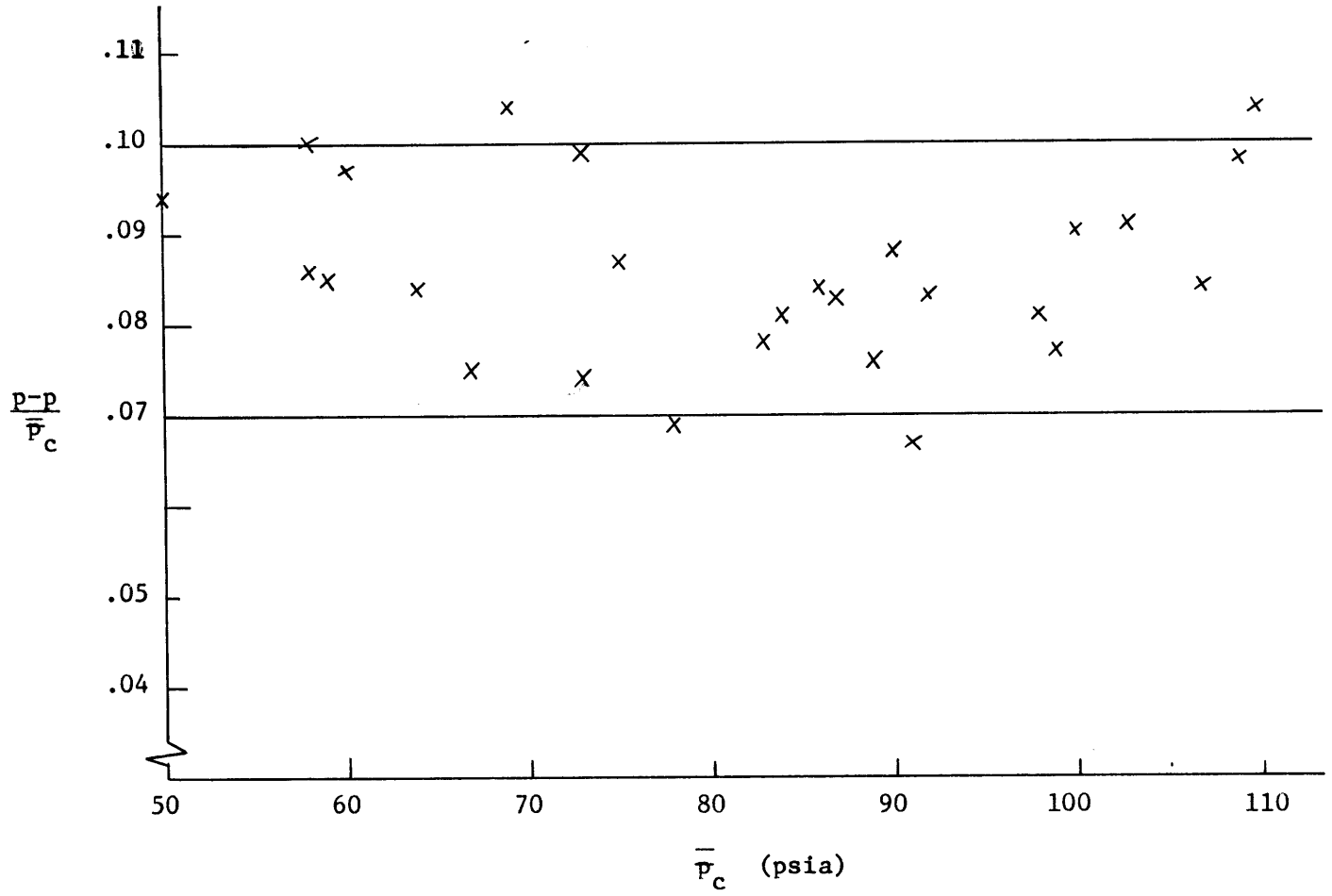

Figure 19 $\frac{p-\bar{p}}{\bar{p}_c}$ vs $\bar{p}_c$ Plot

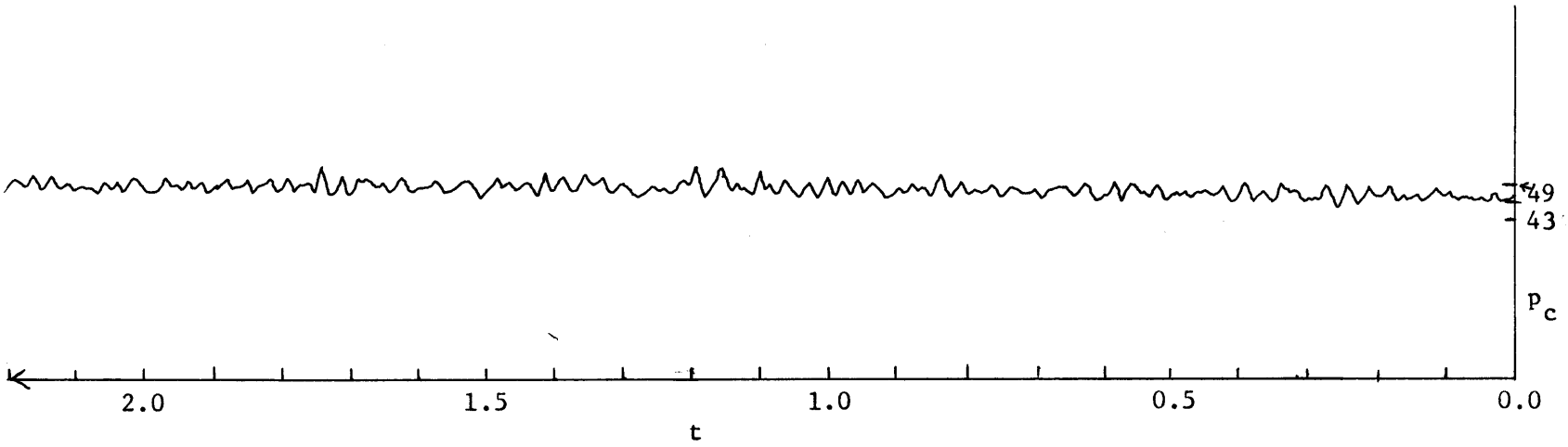

Sample taken from Run 1 for comparison

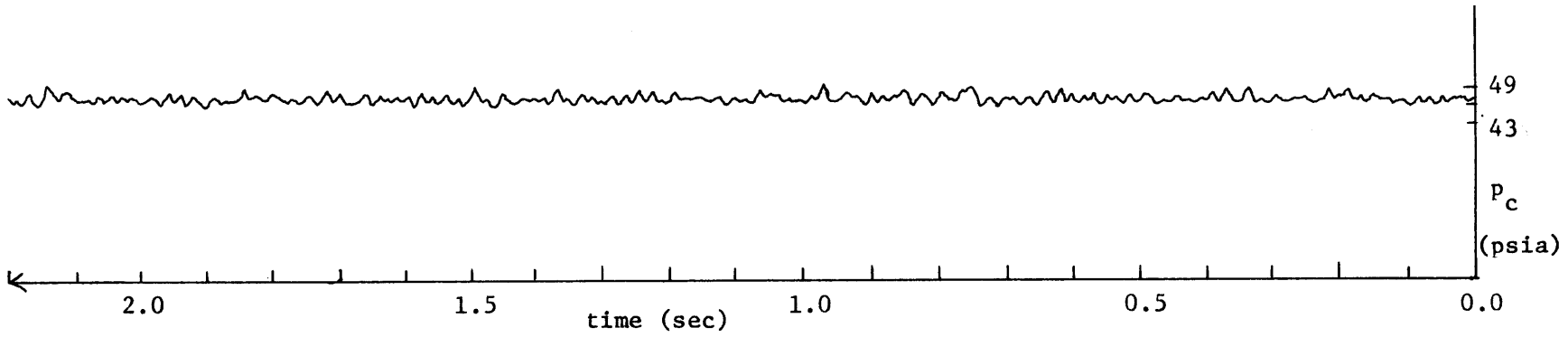

Sample taken from Run 12 - without mixing piece

Figure 20 Mixing piece effect

nozzle (d_t = 0.34 inches) was used for all runs. Also, the leak around the shaft in the control flow oscillator box merely served to add a steady bias flow to the unsteady flow with the pulsing superimposed on top.

Figure 21 shows the behavior of the chamber pressure (the same at both ends of the chamber) without combustion but with oxygen flow. Data from these traces are given in Table 3. The top five show the response for different motor speeds with both steady and unsteady control flow. The bottom trace shows the behavior without the oxygen flow. Variations in figure 21(a) are due to a beating of the chamber pressure oscillations with the 60 cps standard A.C. noise in the recorder trace. The time constant of the decays on the edges of the plots was determined by how fast I turned on the ball valve to admit oxygen. Other tests showed that if the orifices in the oscillator box were not sonic, there was a very significant amount of noise introduced as opposed to the behavior in figure 21(a-f). The vortex valve assembly itself added some noise to the pressure oscillations, but the total was practically indistinguishable from the fluctuations without the valve assembly.

The first conclusion, then, is that the chamber pressure can be driven at a given frequency without combustion. The next question is whether it works with combustion, and how well.

It is obvious that as the frequency increases, the pulsing magnitude decreases significantly. The cause for this is that as the oscillator box shaft speed increased, less mass flow was allowed through the shaft and thus the pulse magnitude decreased. This effect was unfortunate since the forcing amplitude was not much larger than the inherent hybrid oscillation for even the lowest possible frequency (~20 cps). The tabulated driving

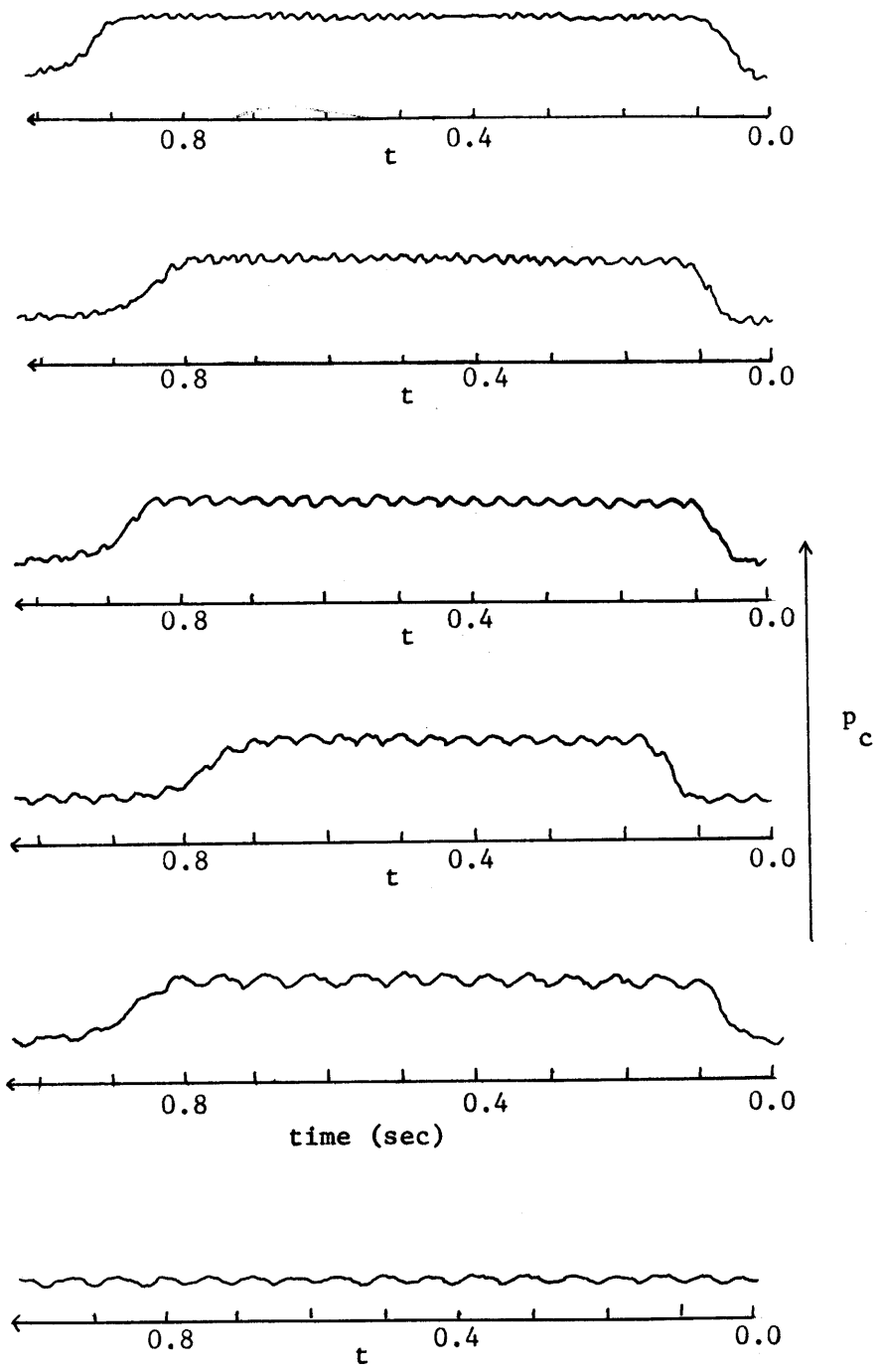

Figure 21 Cold Flow Chamber Pressure Forcing

p_c	p-p	freq.
29	2.9	17.5
29	2.5	25
29	2.2	30
29	1.8	42.2
29	1.4	54.5
psia	psia	sec^{-1}

p_{He} = 185 psig , p_{ox} = 250 psig

Table 3 Cold flow Vortex Valve effectiveness

frequencies were obtained by counting the number of peaks seen in cold flow in a given time period.

The decrease in forcing pressure oscillation amplitude had a number of very interesting repercussions. First, the chamber pressure could be seen to be obviously forced for full steady flow and lower frequencies with combustion as shown in figure 22. Next, it was found that there were little resonance effects achieved at frequencies around that of the instability. If there were any, they are hidden beneath noise, measurement error and decreasing pressure amplitude forcing. One attempt at forcing resonance is shown in figure 23, for a run without steady control flow - just unsteady and leakage. To these is added figure 24, a run at a frequency above the obvious forcing and resonance frequency, where nothing definite at all is visible. The runs which did not use the steady bias flow were generally less useful because they were somewhat less effective, as predicted.

Some miscellaneous observations were also made on the simultaneous pressure variations at each end of the chamber. The pressure variation was again in phase and not in a slosh mode. Also the favorable pressure gradient was decreased by a significant fraction.

The final conclustion is that the chamber pressure can be forced to oscillate at a given frequency using vortex valve control on the exhaust. The limitations encountered here are thought to not be fluid mechanical, but mechanical, and therefore correctable to a point. Whether inherent resonances can be driven is not clear from this apparatus.

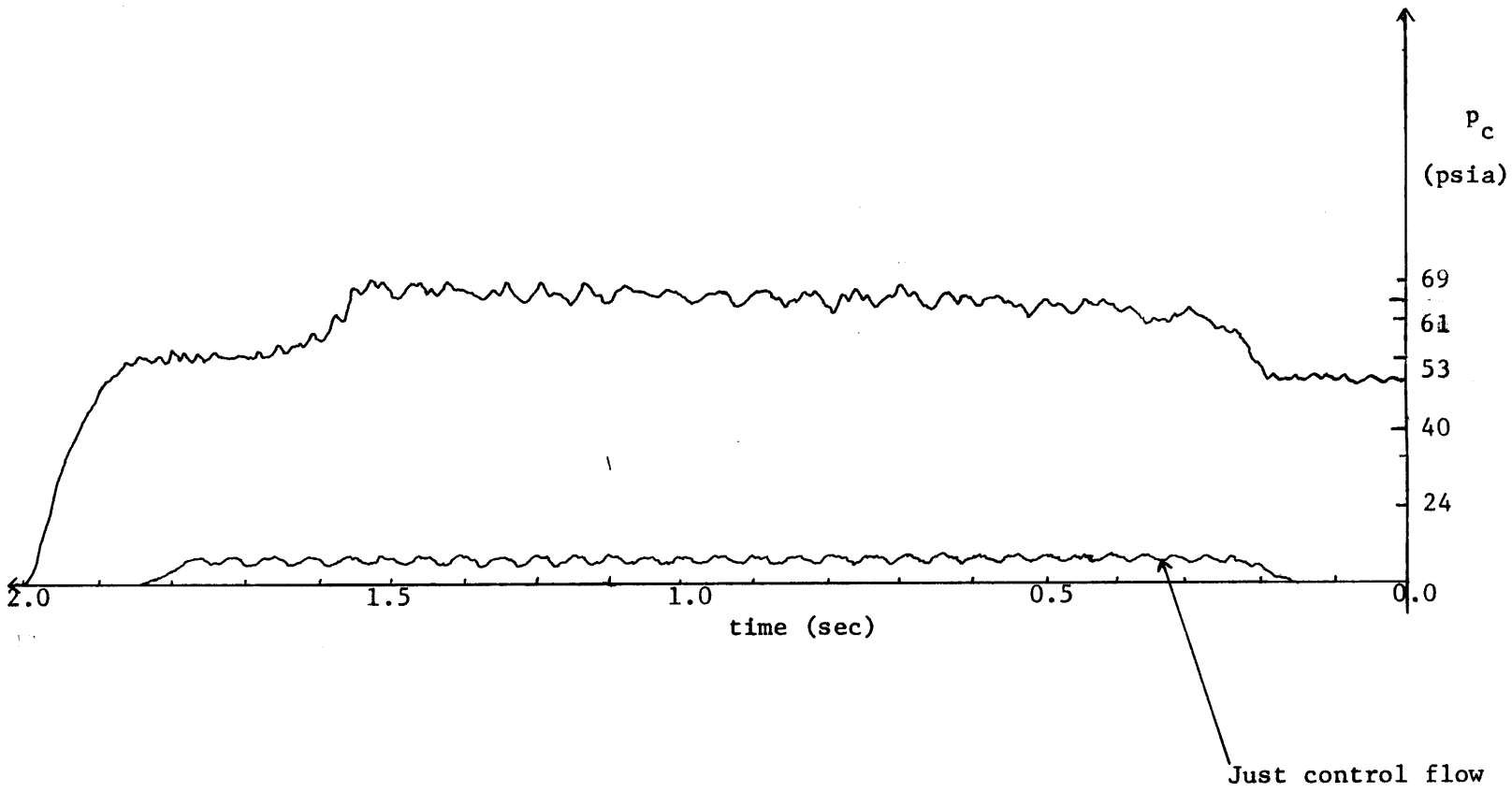

Figure 22 Combustion Chamber Pressure Driving - Low Frequency

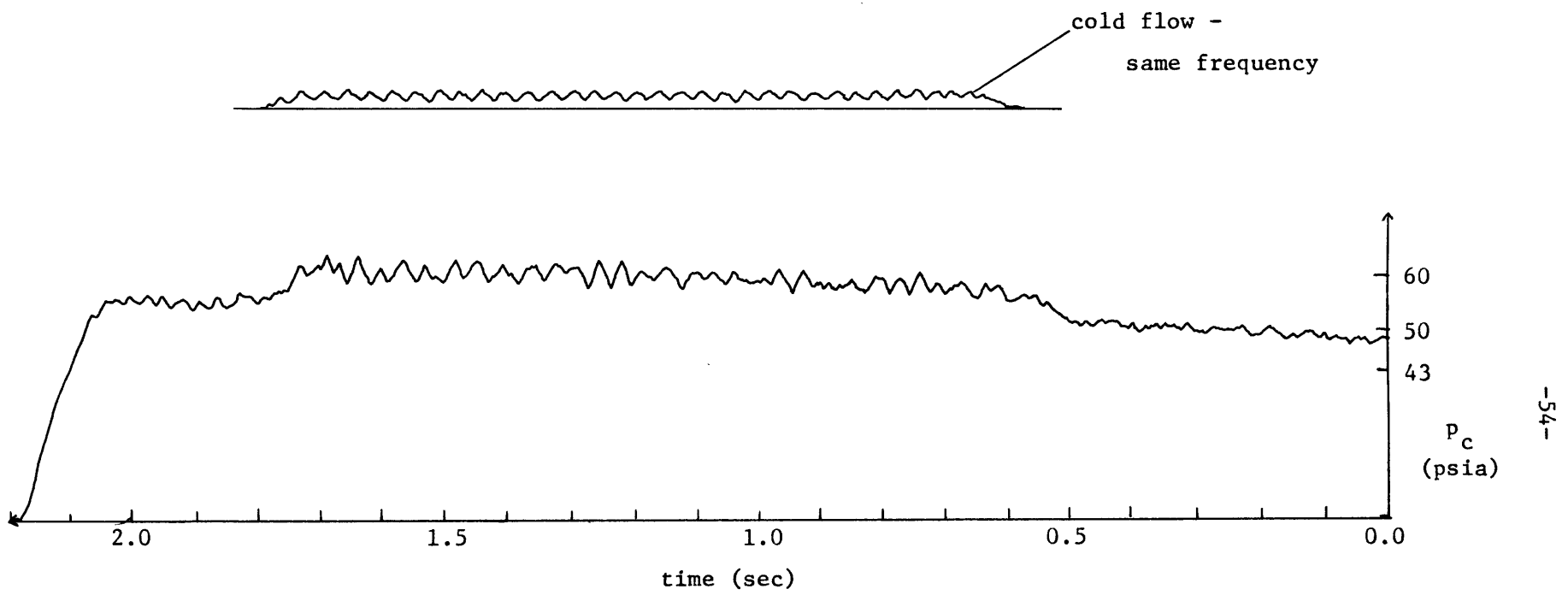

Figure 23 Resonance driving attempt

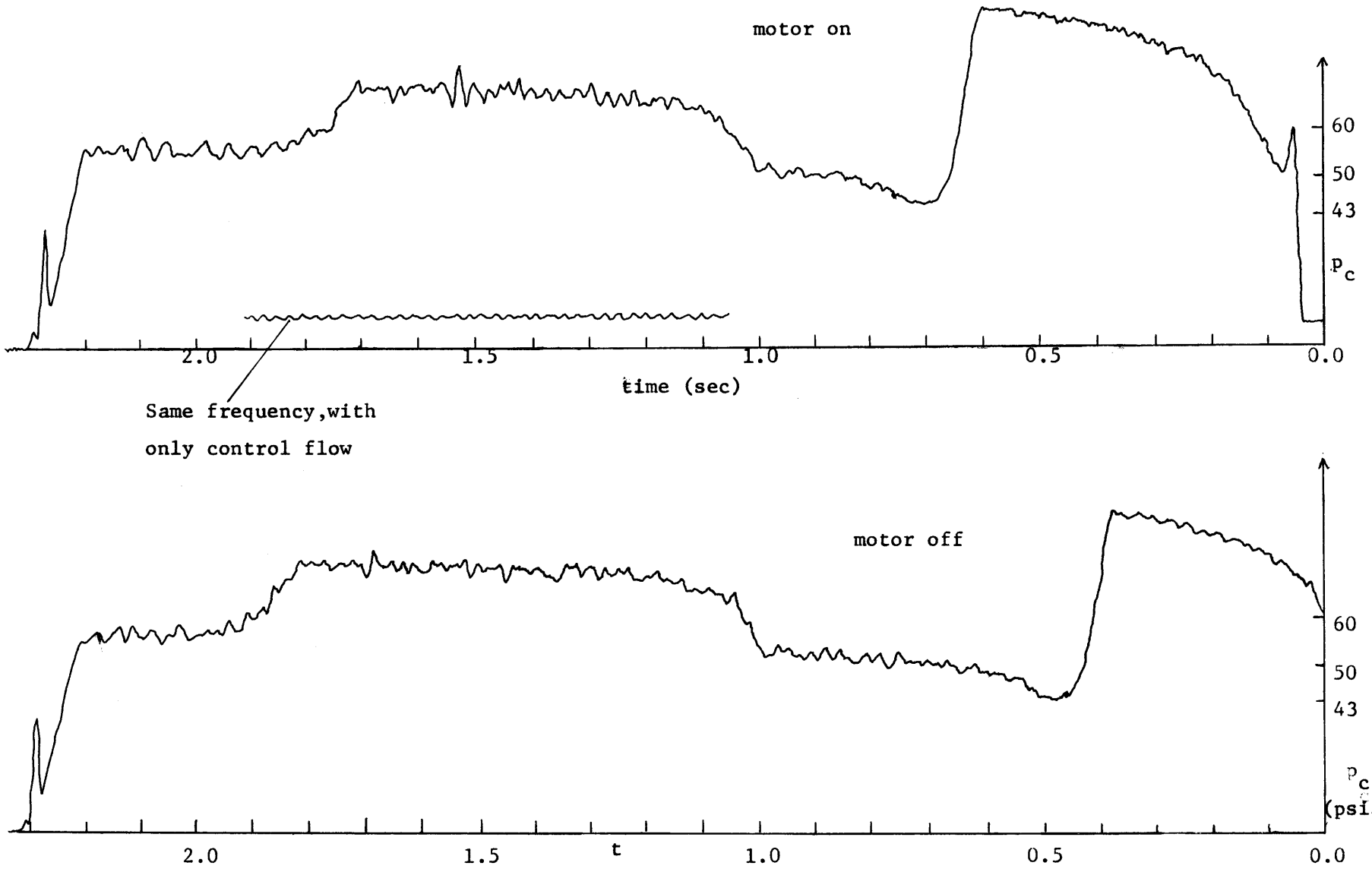

Figure 24 Case of least effective driving

CHAPTER VI

INSTABILITY MECHANISMS

There are a number of different mechanisms that could account for a pressure oscillation inherent in hybrid combustion. All those that could be thought of are explained qualitatively below, and then an attempt is made to isolate the one responsible for the results discussed earlier. These models are not taken from references.

6.1 $\delta\dot{m}_f$ - Vapor Pressure Coupling

The first mechanism assumes vapor pressure equilibrium at the wall. Thus, for a given heat flux to the wall, the regression rate will be determined by the vapor pressure above the fuel surface. Let us now go physically through a cycle proposed by the equilibrium vapor pressure - $\delta\dot{m}_f$ model.

For an initial negative increment in the chamber pressure, since the pressure is constant across the boundary layer, the wall vapor pressure will drop on an acoustic time scale. This is an immediate drop compared to the other time scales. When the wall vapor pressure goes down, the vaporization rate goes up and so does the regression rate. This increase in regression rate slightly reduces the heat flux but the primary effect rests in the increased fuel mass flow.

The additional enthalpy release increases the temperature of the gas in general, and more so downstream behind the nozzle. This, coupled with the additional mass flow through the nozzle, causes a positive increment in chamber pressure. The increase in pressure then causes a decrease in fuel vaporization, which decreases the regression rate,

decreasing $\dot{m}_f$ and the temperature behind the nozzle. As a result, the pressure decreases and the cycle begins again. There are two effects from $\delta\dot{m}_f$: temperature variation and $\delta\dot{m}_f$ itself. Another effect on C^* is a change in the molecular weight due to changes in relative amounts of oxidizer and products.

The time scale of this oscillation will be set by the average transport time of $\delta\dot{m}_f$ from the wall to the point where it burns. This assumes that the depolymerization of fuel and the heat flux to the wall can enable vapor pressure equilibrium to exist when the pressure is decreasing rapidly.

The other extreme from equilibrium is demonstrated by a model of the following form: When the vapor pressure drops, the hot material on the wall surface vaporizes, absorbing heat from the wall alone. Thus the wall regression rate increases and then drops by a larger part until the convective (or radiative) heat flux can heat the surface to the point where the average vaporization rate of fuel is again reached. While the surface is heating, the positive increment in mass flow is transported downstream and eventually burns, increasing the chamber pressure, followed by a larger pressure drop from the drop in the fuel vaporization. A steady oscillation for this model depends on the relative time scales of the surface heating for depolymerization equilibrium and the fuel transport to burning. If the first is about the same as the second, then the larger pressure drop could be coincident with the time at which the surface has reached its averaged state and the cycle can begin again. Since it is very unlikely that the time scales would be this perfect, some kind of beating amplitude would probably occur. This is contrasted with the

steady behavior of the first model. If the first time scale is much longer than the second, no oscillation should occur, the chamber pressure just going to a new level.

6.2 $\delta\dot{m}_f$ - Axial Pressure Gradient Coupling

This model is basically a fluid dynamical one and depends on a chamber pressure gradient oscillation as well as a chamber pressure oscillation. Starting with an average chamber pressure and slight favorable pressure gradient, the chamber pressure is given a positive increment at the downstream end of the charge. This causes the whole pressure to increase on a sonic time scale, but reverse the pressure gradient so it is now slightly adverse. The adverse pressure gradient causes the velocity in the boundary layer to be reversed and separation to occur, decreasing fuel vapor transport away from the wall and the convective heat flux. As a result the regression rate decreases and consequently so does the chamber pressure. As a normal velocity profile reestablishes itself, the pressure gradient is favorable and the regression rate increases, increasing the fuel mass flow which is then transported downstream, burning and increasing the chamber pressure, so the cycle begins again. The pressure gradient will change from favorable to adverse at some point of the chamber pressure increase and change back at or before the time when the pressure amplitude is maximum, so that there is a favorable gradient most of the time. The time scale of this oscillation is the sum of the time it takes to reestablish a "normal" hybrid boundary layer after separation and the transport time from wall to flame zone.

6.3 $\delta\dot{m}_f$ - G Coupling

This model uses G as the coupling between the fuel mass flow perturbation

and the heat release, with the chamber pressure being more incidental. Beginning with a positive perturbation in the fuel mass flow, the chamber pressure and temperature will increase downstream, providing a resistance to the G upstream and thereby decreasing it. This effect on G should be fairly uniform across the boundary layer. The decreased G then decreases $\dot{r}$ which then allows the resistance to G to decrease. G then increases and so does $\dot{m}_f$, so the cycle begins again. The resistance varying is the pressure behind the nozzle and thus the chamber pressure, but here the chamber pressure plays a less important role than before. The G change should be at sonic speeds. This model assumes a preexisting favorable axial pressure gradient that is not driven adverse by the resistance to G. The time scale for this model is again the transport time between the wall and combustion. The effects of the model are both an oscillating chamber pressure and axial pressure gradient (about a favorable average).

6.4 Mechanically Induced

The last possibility is always that the oscillations are just caused by some particularity of construction. In these experiments it is the flow straightener that could cause problems. Some kind of fluctuating shock pattern behind the straightener could be transmitted to give a chamber pressure oscillation. Or perhaps a vortex shedding oscillation off the mixing section.

These are the models for that can qualitatively account for the observed hybrid chamber pressure oscillations. No acceptable model was discovered for radiation pressure coupling. Next, which models fit the behavior observed earlier?

The mechanical models mentioned can be shown to be unlikely. The

The placement of the oxygen sonic orifice, shown below, is such that the flow is almost certainly subsonic before it reaches the flow straightener. The teeth of the tapped hole provide shock holders and a long expansion

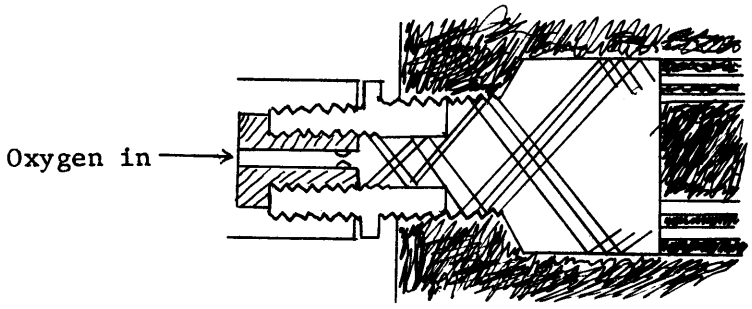

section make shock oscillations unlikely. Furthermore the same shock pattern was present in cold flow runs and no noise like that seen during combustion was observed. If the coupling just occurred during combustion, then the conditions near the nozzle should have a small effect on the shocks, which is contrary to the observed importance of the mixing piece. As for vortex shedding off of the mixing piece, the oscillation was only reduced in amplitude, not removed, by combusting without the protruding parts.

The model proposing an oscillation between favorable and adverse axial pressure gradients is eliminated by the recording of a 12 psia (uncertainty 4 psia) favorable axial gradient, while the chamber pressure peak-to-peak oscillation amplitude was at a maximum of 6-7 psia. This is just not enough to reverse the pressure gradient.

The G coupling model is dismissed by the experimental observation that the oscillation amplitude does not depend on G as it would in this model. This conclusion is made secure by Run 10 where both the chamber pressure and oscillation amplitude decreased by 2/3 while G remained constant. Any G coupling model will have to make the oscillation amplitude independent of G.

This leaves the vapor pressure coupling with the regression rate and the two separate models. However an initial question to answer is how well the models fit with order of magnitude estimates. The fuel mass flow rate is only 20% of the total mass flow and the models speak of a perturbation in this fuel mass flow. Can this small a change in mass flow result in the observed behavior?

The basic perturbation equation is taken from the relation for a sonic throat.

$$p_c = \frac{C^*_c}{A_{tc}} (\dot{m}_{ox} + \dot{m}_f) \tag{6.1}$$

Perturbing this in $\dot{m}_f$ and C^*_c and adding equation (5.2).

$$\delta p_c = \left(\frac{A_{tox}}{A_{tc}}\right)\left(\frac{p_{ox}}{C^*_{ox}}\right) \delta C^*_c + \left(\frac{\dot{m}_f}{A_{tc}}\right) \delta C^*_c + \left(\frac{C^*_c}{A_{tc}}\right) \delta \dot{m}_f \tag{6.2}$$

For a plexiglas-oxygen system, the molecular weight of the combustion products are not far different from that of oxygen, so the effect of changing molecular weight is neglected. This effect, if considered, would increase δp_c since the average molecular weight of the combustion products is less than oxygen.

The following values were then used, taken from Run 5:

$d_t = 0.100$ in., $d_{tc} = 0.36$ in., $\gamma_c = 1.35$, $p_{ox} = 300$ psia, $C^*_{ox} = 1340$ ft/sec

$C^*_c = \frac{p_c A_{tc}}{\dot{m}_{tot}} = 4250$ ft/sec, $M_c \simeq 25 \frac{\text{lb}}{\text{lb-mole}}$, $\bar{\dot{m}}_f = 3.64 \times 10^{-4}$ slugs/sec

Thus: $\delta p_c = 2.15 \times 10^{-2} \delta C^*_c + 4.16 \times 10^{4} \delta \dot{m}_f$

Also $C^*_c = 4250$ ft/sec implies $T_c = 2020°K$ which is not unreasonable. A $\delta \dot{m}_f$ of 10% $\dot{m}_f$ and a δT_c of 50°K gives a $\delta p_c = 2.5$ psi. This is low by a factor of two or three for the maximum amplitude but is the right order

of magnitude. Furthermore, doing an even cruder calculation on the heat release from a $\delta\dot{m}_f = 10\%\dot{m}_f$ gives the same order of magnitude as δT_c.

The basic model of a mechanism for a change in p_c from a change in $\dot{m}_f$ is then reasonable. It also coincides well with the observation of the importance of the mixing piece; since this enables complete combustion, so that the large molecular weight of the unburned fuel $\delta\dot{m}$ will not cancel out the δT_c effect in C_c^*. Next the time scale of the model can be checked with experiment. A characteristic time scale can be calculated by estimating the density of the oxidizer just after the flow straightener when it is fairly cool. This, coupled with the experimental value of G will give a chamber axial velocity and thus a time scale for transport. This is on the order of 5 milliseconds. The time scale of the transport of $\delta\dot{m}_f$ from the wall to the point of combustion will be an order of magnitude longer than this, however, since $\delta\dot{m}_f$ starts with a zero axial velocity and must be accelerated downstream. So the time scale ($\simeq$ 3 ms), also appears reasonably coincident with the observed oscillation (40cps = 2.5ms).

Next we can look at the wall vapor pressure coupling.

The vapor pressure equilibrium model would be possible except for the fact that in this case the steady state regime of operation is not pressure dependent. The model implicitly requires this effect in the oscillation mechanism, and thus in the steady state. So we are left with one final model. It does not imply a pressure dependency in the regression rate except in the sense of rapid variations with respect to the heat flux.

The non-equilibrium wall vaporization model appears to be the correct explanation. One more point that could possibly be in its favor is that it predicts a beating type of pressure amplitude variation. this beating

could be the dominant cause of the randomness in amplitude that was observed and would indicate an inherent difficulty in forcing resonance by driving the amplitude at one frequency. The randomness in amplitude, however, is more likely due to a number of different, generally turbulent effects.

There are at least two experiments suggested by this model. One is a better attempt at forcing resonance. Another is that the $\delta\dot{m}_f$ appears to be significant enough fraction of $\dot{m}_f$ so that it might be possible to detect light pulses from the flame zone coincident with the pressure oscillation. These would be too fast to be seen with the eye, but could easily be measured with a photodiode, for example, and correlated if they did indeed exist.

CHAPTER VII

CONCLUSIONS

The plexiglas-oxygen system that was used as a hybrid test device has a regression rate behavior that primarily obeys the standard heat transfer limited theory. For lower flow rates, however, pressure dependent effects here ascribed to radiation are observed.

Vortex valve exhaust driven chamber pressure oscillations are definitely attainable. The mechanical device used limited the possible driving amplitudes but this is not a basic limitation on the method. Perhaps due to this limitation, no significant resonance driving with existing hybrid pressure oscillations was observed, although the driving was close to the proper frequency.

These inherent pressure oscillations are found to be strongly dependent on the existence of a final mixing section and not on G. They are not low frequency slosh modes either. Of the models proposed, only one was found to agree well with the experimentally observed pressure oscillations. This is a nonequilibrium coupling between wall vapor pressure and fuel mass flow. The variation in mass flow then causes variations in gas properties behind the chamber nozzle, resulting in a change in chamber pressure. This effect is the right order of magnitude and the explanation of the chamber pressure oscillation seems to be satisfactory.

Tne most significant improvement that can be made in the experimental apparatus used, is increasing the amplitude of the pulsed control into the vortex valve. This should be easily accomplished.

APPENDIX A

ERROR ESTIMATES

Sources of Error:

1) Strip Chart Recorder: 2% of full deflection
2) Pressure Transducer calibration error
3) Strip Chart reading error
4) t_b reading errors - uncertainty of ignition time
5) Weighing errors
6) Errors from non-uniform fuel charges
7) Averaging errors
8) Plexiglas chemical composition differences
9) Mistakes

Error Estimates:

1), 2), 3) $\bar{p}_c$ error $\simeq$ 10%, p_{ox} error $\simeq$ 6-7%

$$\text{error} \propto \frac{1}{\bar{p}_c}, \frac{1}{p_{ox}}$$

4) t_b good to $\pm$ .2 sec ; $\simeq$ 6%

$$\text{error} \propto \frac{1}{t_b}$$

5) weighing errors - $\pm$ .1 gram ~2%

$$\text{error} \propto \frac{1}{M_L}$$

Conclusion:

$\dot{m}_f$ error $\simeq$ 8% total, $\pm$ 4%

$\bar{\dot{r}}$ error $\simeq$ 10% total, $\pm$ 5%

RUN	before d_t	after d_t	p_c max	t max	p_c initial	p_c final
1	.339	.341	50	8.5	45	50
2	.341	.386	59	8.0	53	46
3	.337	.367	74	7.1	68	65
4	.337	.345	80	7.8	78	85
5	.339	.377	92	5.4	85	78
6	.306	.314	60	9.0	54	58
7	.315	.331	69	8.5	62	64
8	.303	.323	90	6.5	81	83
9	.305	.309	100	8.0	92	98
10	.305	~.4	109	4.5	101	47
11	.305	.305	110	9.5	99	110
12	.382	.382	≈51	≈8	43	≈47
units	inches	inches	psia	seconds	psia	psia

Table 4 Measurements for averaging

APPENDIX B

MECHANICAL DRAWINGS

(drawings are full scale)

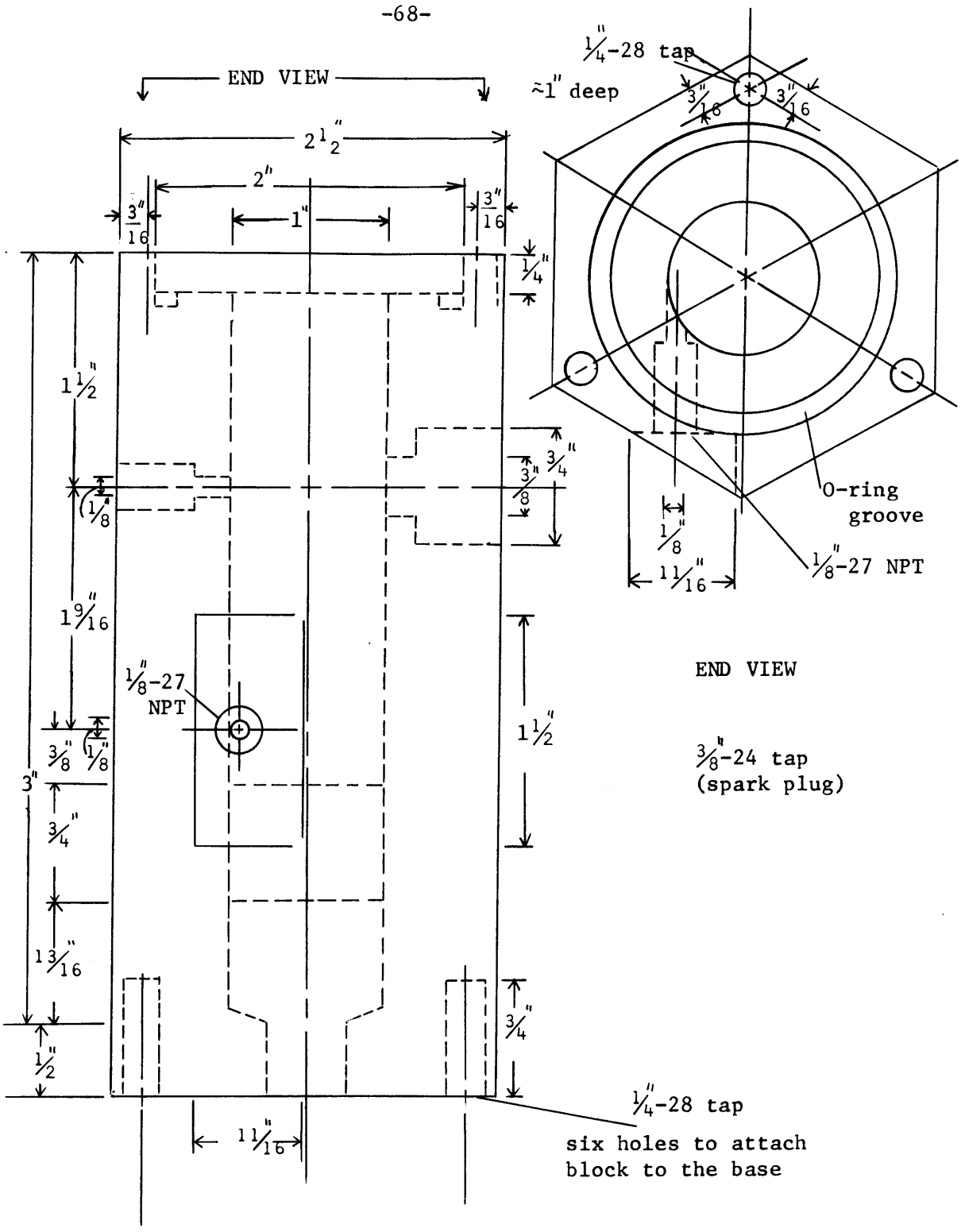

IGNITION BLOCK

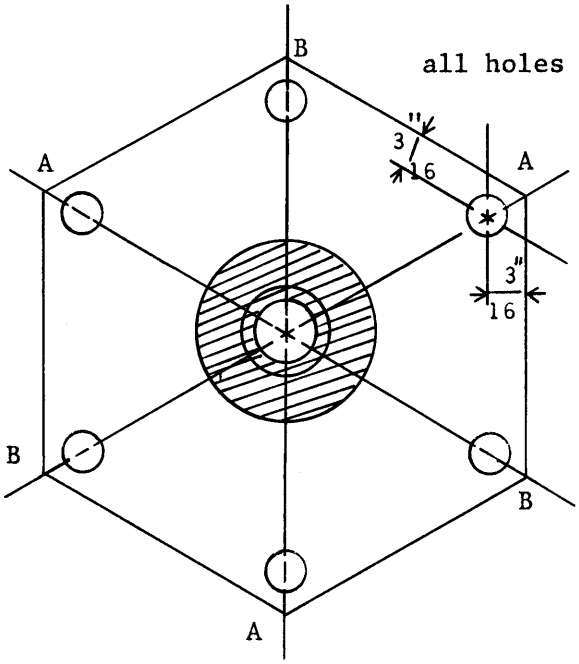

all holes centered identically

END VIEW

END VIEW

A - connecting rod holes
I drill (¼" rods)
through block

B - bolt holes, through
end piece and ¾" deep
in block - ¼" bolt
28 threads/in.

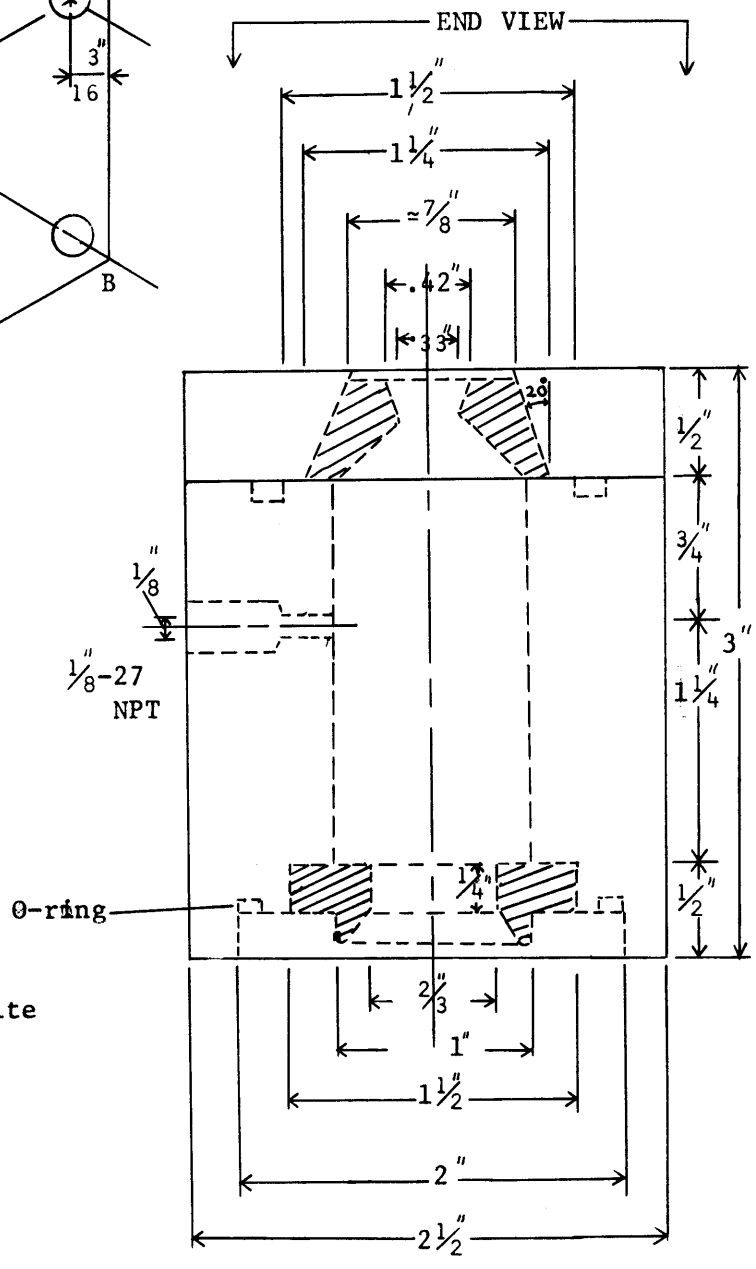

indicates graphite

All O-rings: grooves;

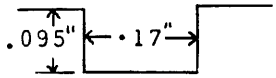

thickness = ⅛"

NPT = National Pipe Tap

MIXING BLOCK, NOZZLE & END PIECE

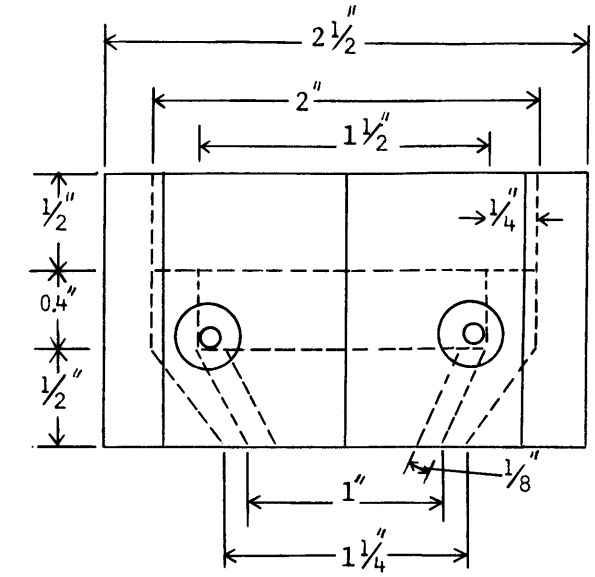

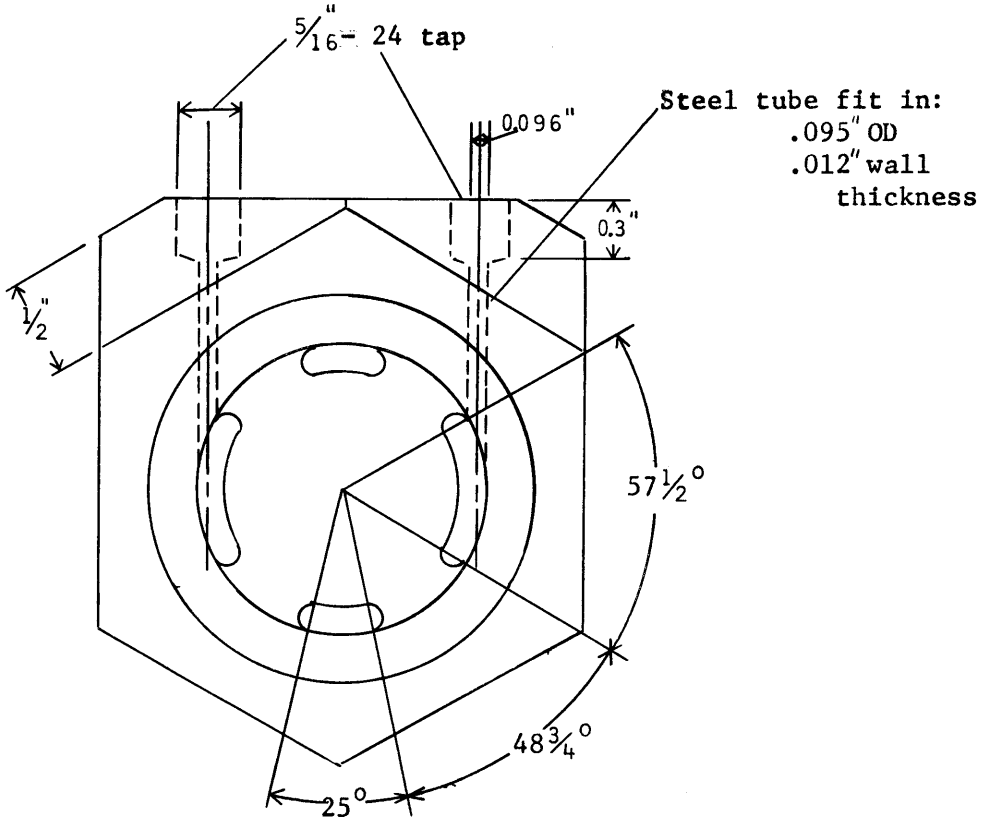

VORTEX VALVE BLOCK

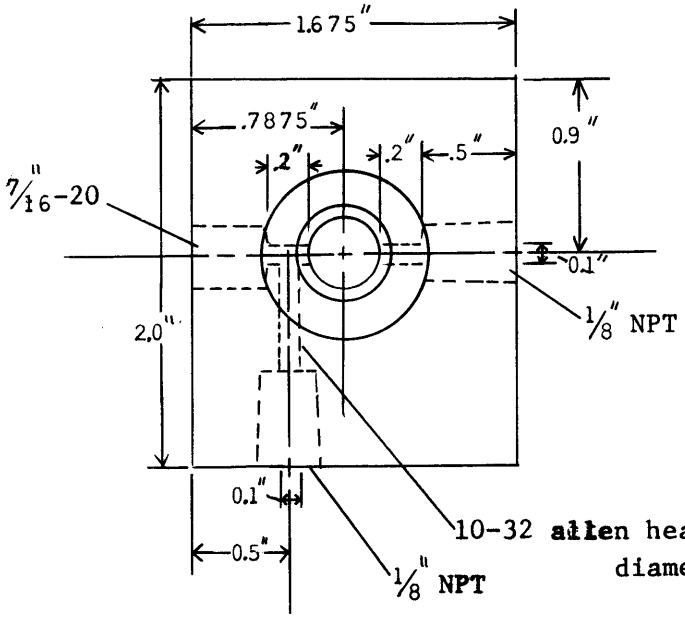

Top View

ball bearing case recess

bearing case is 7/8"OD x 1/4"

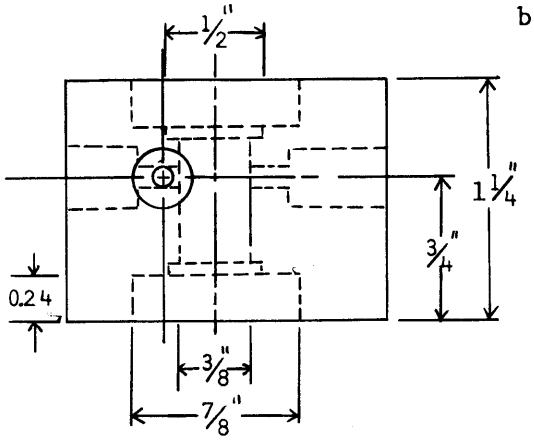

Front View

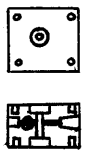

Not included: 4 holes in the corners of the block on both sides for screws to secure top and bottom, 1/8" aluminum sealing plates.

OSCILLATOR BLOCK

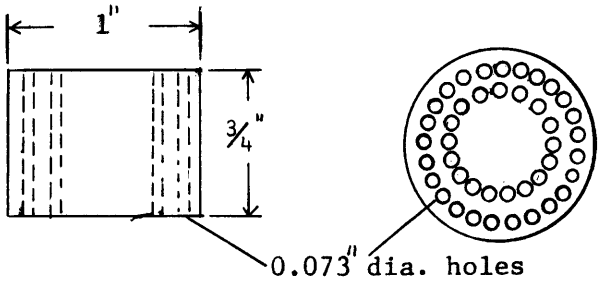

FLOW STRAIGHTENER

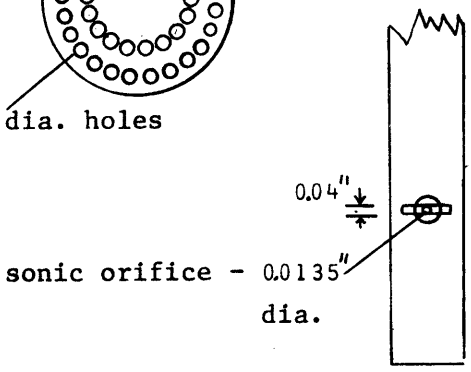

CONTROL FLOW CONNECTOR

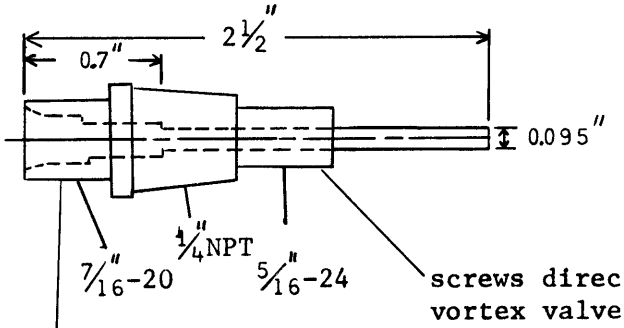

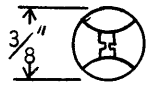

OSCILLATOR
BLOCK
SHAFT

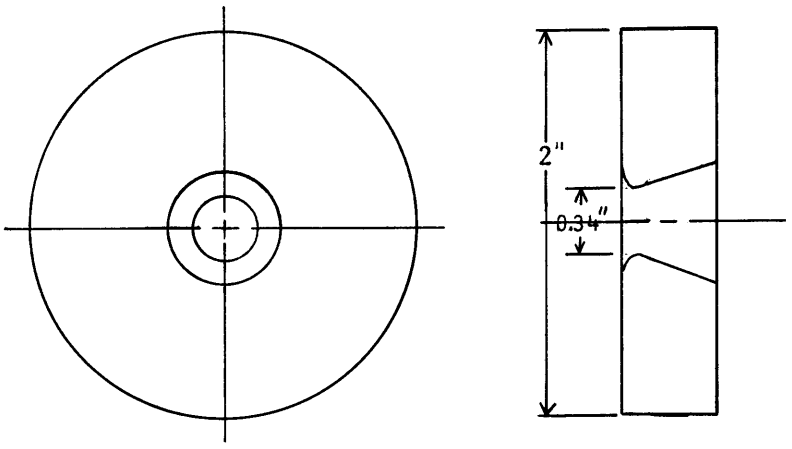

VORTEX VALVE NOZZLE BLOCK

REFERENCES

1. Hill, Philip G., and Peterson, C. R., Mechanics and Thermodynamics of Propulsion, Addison-Wesley, Reading, Mass., 1965, pp. 64-97.

2. Kumar, R. N., "Some Considerations in Hybrid Combustion," Doctoral Thesis, M.I.T., 1971

3. Lees, L., "Convective Heat Transfer with Mass Addition and Chemical Reactions," Combustion and Propulsion, Third AGARD Colloquium, Pergamon, 1958, pp. 451-497.

4. Lewellen, W. S., Burns, W. J., and Strickland, H. J., "Transonic Swirling Flow," AIAA Journal, vol. 7, no. 7, July 1969, pp. 1290-1297.

5. Marxman, G. A., "Combustion in the Turbulent Boundary Layer on a Vaporizing Surface," Tenth Symposium on Combustion, The Combustion Institute, 1965, pp. 1337-1349.

6. Marxman, G. A., Wooldridge, C. E., and Muzzy, R. J., "Fundamentals of Hybrid Boundary Layer Combustion," Progress in Astronautics and Aeronautics, vol. 13, Academic Press Inc., New York, 1964, pp. 485-522.

7. Marxman, G. A., and Gilbert, M., "Turbulent Boundary Layer Combustion in the Hybrid Rocket," Ninth Symposium (National) on Combustion, Academic Press, 1963, pp. 371-382.

8. Smoot, L. D., and Price, C. F., "Regression Rate Mechanisms of Non-Metalized Hybrid Fuel Systems," AIAA Preprint 65-56, 1965.

9. Stickler, D. B., and Kumar, R. N., "Polymer Degradation Theory of Pressure Sensitive Hybrid Combustion," Thirteenth Symposium on Combustion, the Combustion Institute, 1970, pp. 123-136

10. United Technology Center, Investigation of Fundamental Phenomena in Hybrid Propulsion, vol. 1, Final Technical Report, Sunnyvale, California, Nov. 1965.

11 Walsh, R. F., "Investigation of a Solid Propellant Rocket Motor Modulated by a Fluid Vortex Valve," Masters Thesis, M.I.T., September 1969